




ARTICLE

Site-specific regulation of Th2 differentiation within lymph node microenvironments

Miranda R. Lyons-Cohen¹, Elya A. Shamskhou¹, and Michael Y. Gerner¹

T helper 2 (Th2) responses protect against pathogens while also driving allergic inflammation, yet how large-scale Th2 responses are generated in tissue context remains unclear. Here, we used quantitative imaging to investigate early Th2 differentiation within lymph nodes (LNs) following cutaneous allergen administration. Contrary to current models, we observed extensive activation and “macro-clustering” of early Th2 cells with migratory type-2 dendritic cells (cDC2s), generating specialized Th2-promoting microenvironments. Macro-clustering was integrin-mediated and promoted localized cytokine exchange among T cells to reinforce differentiation, which contrasted the behavior during Th1 responses. Unexpectedly, formation of Th2 macro-clusters was dependent on the site of skin sensitization. Differences between sites were driven by divergent activation states of migratory cDC2 from different dermal tissues, with enhanced costimulatory molecule expression by cDC2 in Th2-generating LNs promoting prolonged T cell activation, macro-clustering, and cytokine sensing. Thus, the generation of dedicated Th2 priming microenvironments through enhanced costimulatory molecule signaling initiates Th2 responses *in vivo* and occurs in a skin site-specific manner.

Introduction

Upon activation, naïve CD4 T cells differentiate into distinct helper cell lineages with specific effector functions tailored to eliminate different classes of pathogens. Th2 cells provide defense against parasitic helminth infections and promote tissue repair, but when inappropriately activated, can cause allergic disease or asthma (Walker and McKenzie, 2018). Much work has gone into understanding the cellular and molecular mechanisms driving early Th2 differentiation, collectively resulting in the quantitative and qualitative models, which are also somewhat divergent from how other T helper cell lineages are thought to be generated (van Panhuys, 2016; van Panhuys et al., 2014).

The quantitative model posits that the signal strength sensed during initial T cell activation is a major factor regulating T helper cell polarization. Th2 differentiation has been suggested to involve decreased T cell receptor (TCR) signaling, either through reduced TCR affinity, lower levels of peptide MHC (pMHC) complexes presented by antigen-presenting cells (APCs), or through limited sensing of costimulatory molecules (Bhattacharyya and Feng, 2020; van Panhuys, 2016; van Panhuys et al., 2014). Reduced signaling is thought to decrease the longevity of T cell-DC interactions, thus minimizing the ability of T cells to respond to inflammatory cytokines from DCs and ultimately promoting an endogenous program of Th2

polarization (Mempel et al., 2004; van Panhuys et al., 2014; Zhu et al., 2012). Confounding this model is the notion that generally all *in vivo* responses involve polyclonal T cell populations with diverse TCR affinities, yet Th2 cells are not generated in all inflammatory contexts. Additionally, enhanced exposure to costimulatory molecules has been positively and not negatively associated with Th2 differentiation (Gause et al., 1997; King et al., 1995; Liu et al., 2004; Rulifson et al., 1997; Tao et al., 1997; van Rijt et al., 2004). It is also not clear how low-grade stimulation elicits large-scale *in vivo* Th2 responses as observed during helminth or allergen exposure, especially given that both result in maturation of cDCs and significant costimulatory molecule expression (Besnard et al., 2011; Hung et al., 2020; Ito et al., 2005; Stanbery et al., 2022).

In addition to quantitative signal strength-based factors, qualitative sensing of polarizing cytokines is important for T cell differentiation *in vivo*. However, unlike other helper cell lineages, Th2-promoting cytokines do not appear to operate in a typical “signal 3” fashion through production by APCs (León, 2023). Interleukin (IL)-4 is critical for Th2 differentiation both *in vitro* and *in vivo*, but this cytokine is not produced by cDCs and the exact cellular source(s) of IL-4 in LNs remains ill-defined (León, 2023; Walker and McKenzie, 2018). Notably, recently

¹Department of Immunology, School of Medicine, University of Washington, Seattle, WA, USA.

Correspondence to Michael Y. Gerner: gernermy@uw.edu.

© 2024 Lyons-Cohen et al. This article is distributed under the terms of an Attribution–Noncommercial–Share Alike–No Mirror Sites license for the first six months after the publication date (see <http://www.rupress.org/terms/>). After six months it is available under a Creative Commons License (Attribution–Noncommercial–Share Alike 4.0 International license, as described at <https://creativecommons.org/licenses/by-nc-sa/4.0/>).

activated T cells can produce IL-4 after TCR stimulation independently of the Th2 lineage-defining transcription factor, Gata binding protein 3 (Gata3), and paracrine delivery of IL-4 between activated T cells can be sufficient for Th2 differentiation (Chu et al., 2014; Noben-Trauth et al., 2000, 2002; Paul and Zhu, 2010). Similarly, T cell-derived IL-2, also produced downstream of T cell activation, is necessary for Th2 response formation in vivo (Hondowicz et al., 2016; Paul and Zhu, 2010), and this cytokine is again delivered via the paracrine exchange between activated T cells and not provided by APCs (DiToro et al., 2018; Sabatos et al., 2008).

Moreover, not all cDC populations have equivalent capacities to induce Th2 responses. Following barrier tissue damage, locally released alarmins induce the activation of cDC2s, including cells expressing CD301b and variegated levels of Sirpa/CD11b expression (Besnard et al., 2011; Kumamoto et al., 2013). Activated cDC2s in turn migrate into draining LNs, where they can induce Th2 responses (Ito et al., 2005; Gao et al., 2013; Kumamoto et al., 2013; Plantinga et al., 2013; Williams et al., 2013; Ochiai et al., 2014; Tussiwand et al., 2015). cDC2s, however, are also highly plastic, and based on the nature of the stimulus can generate diverse helper lineages, including T follicular helper (Tfh), Th1, and Th17 cells (Connor et al., 2017; Hilligan et al., 2020; Krishnaswamy et al., 2017; Li et al., 2016), and the exact molecular mechanisms of how these cells promote Th2 responses during type-II inflammation remain unknown. cDC1s on the other hand constitutively secrete IL-12 and inhibit Th2 responses, instead promoting Th1 and CD8 T cell immunity (Conejero et al., 2017; Everts et al., 2016). Optimal Th2 differentiation thus likely involves both selective engagement with appropriately activated cDC2 and avoidance of cDC1 populations. How such selectivity is achieved in vivo is unknown, although recent quantitative imaging studies demonstrated that different cDC subsets are non-equivalently spatially distributed within LNs, which could allow for preferential engagement versus avoidance of specific DC subsets by responding T cells in distinct tissue compartments (Germer et al., 2015). Indeed, during type-I inflammation, the spatial positioning of specific innate subsets, including monocytes and activated cDCs, establishes the formation of dedicated microenvironments in the deep T cell zone to generate effector Th1 and CD8 T cell responses (Groom et al., 2012; Leal et al., 2021). In contrast, CD301b⁺ cDC2s predominantly localize at the T-B border, a location where early Th2 cells have also been noted (Kumamoto et al., 2013; León et al., 2012; Randolph et al., 1999; Stoltzfus et al., 2020). This suggests an additional underexplored spatial component of Th2 differentiation in which LN microenvironments populated by appropriately instructed myeloid subsets drive T cell differentiation toward distinct helper lineages.

Here, we used quantitative microscopy to investigate the early stages of in vivo Th2 differentiation after cutaneous administration of the allergen, papain, and other type-II stimuli, as well as compared these responses to Th1 differentiation with TLR agonist immunization. In contrast to the predicted limited cellular activation in Th2 settings, we observed enhanced T cell signaling and extensive clustering, here termed “macro-clustering,” of early differentiating Th2 cells, which primarily

occurred near the T-B border of the LN paracortex. Macro-clustering was integrin-mediated and was associated with enhanced cytokine signaling, suggesting that the spatial proximity of activated T cells enables optimized cytokine exchange for Th2 differentiation. T cell signaling and clustering behavior were also distinct from that seen with adjuvant-induced Th1 responses. Surprisingly, the formation of Th2 responses was highly dependent on the specific site of type-II agonist administration, with footpad-delivered stimuli eliciting markedly reduced Th2 responses as compared with other skin sites, but without compromised ability to elicit Th1 differentiation. Differences across the sites were driven by divergent activation states of migratory cDC2, with enhanced costimulatory molecule expression by cDC2 in Th2-inducing LNs leading to T cell macro-clustering, cytokine signaling, and Th2 differentiation. Collectively, our findings demonstrate that enhanced costimulation and integrin-driven prolonged T-DC crosstalk promote T cell macro-clustering and generate LN microenvironments that drive Th2 response formation in vivo. Our data also support the emerging notion that the generation of T cell responses is heavily impacted by upstream barrier tissues (Ataide et al., 2022; Poholek, 2021), also raising questions on the mechanisms leading to divergent responses across skin sites and having implications for allergic disease development.

Results

Generation of Th2 microenvironments in skin draining LNs

To examine the early processes governing in situ Th2 differentiation, we crossed ovalbumin (OVA)-specific TCR-transgenic OT-II mice to 4get-GFP IL-4 mRNA reporters to generate 4get-GFP OT-II mice (4get-GFP.OT-II) on a CD45.2 congenic background (Mohrs et al., 2001). We then adoptively transferred naïve 4get-GFP.OT-II CD4 T cells into CD45.1⁺ recipient B6 mice, administered papain plus OVA intradermally in the ear pinnae 1 day later, and examined the localization and phenotype of activated OT-II cells in auricular (Au) draining LNs 2–3 days after immunization using quantitative multiparameter microscopy. Papain is a cysteine protease and a clinically relevant allergen in humans and mice that drives robust induction of type-II immunity after cutaneous administration (Kumamoto et al., 2013). CD62L blocking antibody was also administered 6 h after immunization to minimize the impact of asynchronous activation of naïve T cells recruited into LNs late into the response (Gérard et al., 2013). We observed the formation of extensive macro-clusters of OT-II cells located primarily at the T-B border of draining LNs (Fig. 1 A), and the clustered cells expressed high levels of interferon regulatory factor 4 (IRF4) and Ki67, indicative of activation and proliferation (Fig. 1, A and B, region 1 inset). Cells within the clusters also expressed high quantities of the Th2 lineage-defining transcription factor, Gata3, and were positive for the 4get-GFP reporter signal, indicating IL-4 mRNA transcription. In contrast, fewer activated OT-II cells outside the macro-clusters expressed Gata3 and 4get-GFP (Fig. 1, A and B, region 2 inset), suggesting that the macro-clusters represented regions where T cells underwent their earliest stages of Th2 lineage commitment detectable with this

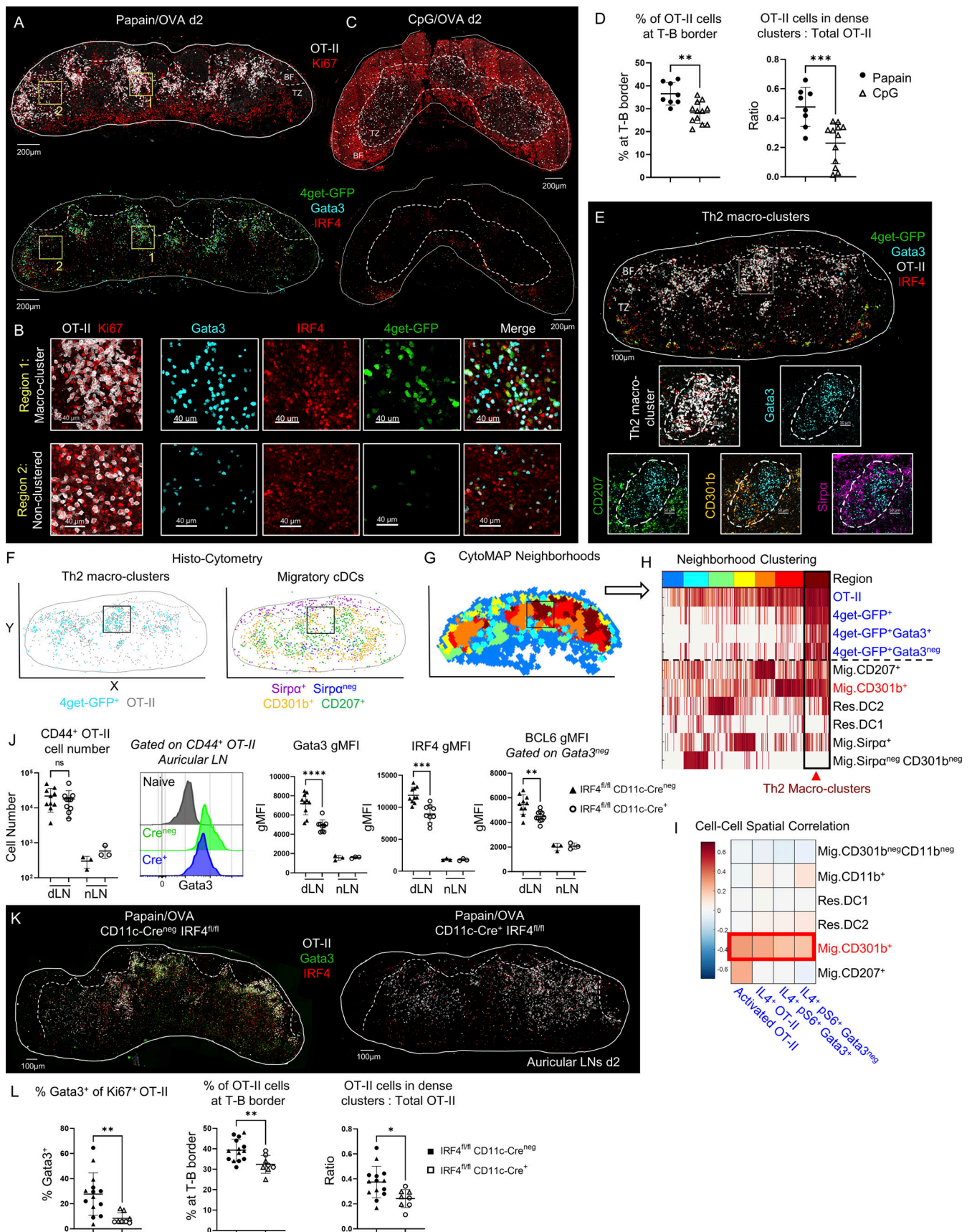


Figure 1. **Generation of Th2 microenvironments in draining LNs.** (A–I) Naive CD45.2 4get-OT-II T cells were transferred to CD45.1 mice and injected with the indicated adjuvants plus OVA in the ear pinnae. Mice were treated intraperitoneally with α -CD62L blocking antibody 6 h after immunization and dLNs were

harvested and assessed by confocal imaging and histocytometry at 48 h. **(A)** Representative images depicting Th2 macro-clustering at the T–B border in Papain OVA immunized dLNs. **(B)** Macro-clustered and non-clustered regions are highlighted in insets with the indicated markers shown. Gata3 signal is masked outside of Ki67⁺IRF4⁺ activated cells for visual clarity. **(C)** Representative images depicting OT-II responses in dLNs after CpG OVA immunization. **(D)** Histocytometry analyses of OT-II localization at the T–B border and the ratio of macro-clustered versus total OT-II cells. **(E–I)** Tissue sections were analyzed for the association of Th2 cells with myeloid cells using CytoMAP. **(E)** Representative confocal image depicting Th2 macro-clusters and Gata3 staining with different myeloid cell markers. **(F)** Spatial distribution analysis of indicated myeloid cell and activated (IRF4⁺Ki67⁺) T cell subsets. **(G)** 50- μ m raster scan neighborhoods of a representative dLN were plotted on a X,Y positional plot and color-coded using neighborhood clustering, as shown in panel H. **(H)** Heatmap demonstrating the cellular composition for each neighborhood cluster (color depicted at the top). Th2 region (dark red) enriched with CD301b⁺ DCs is highlighted (arrowhead). **(I)** Cell–cell spatial correlation of the indicated T cell subsets and myeloid cell populations. **(J–L)** Naïve CD45.1 OT-II T cells were transferred into CD11c-Cre⁺ IRF4^{fl/fl} or CD11c-Cre⁻ IRF4^{fl/fl} CD45.2 mice and then immunized with papain OVA in the ear pinnae, treated with α -CD62L blocking antibody at 6 h, and dLNs were harvested and assessed by flow cytometry or confocal microscopy at 48 h. **(J)** CD44⁺ OT-II cell number is shown with representative histogram and quantification of Gata3 gMFI, IRF4 gMFI, and BCL6 gMFI of CD44⁺ OT-II. **(K)** Representative images depicting OT-II macro-clustering in Cre⁺ and Cre⁻ dLNs with the indicated markers shown. **(L)** Histocytometry analyses of Gata3 expression, OT-II localization at the T–B border, and the ratio of macro-clustered versus total OT-II. Data shown represent one independent experiment with at least $n = 8$ independently immunized lymph nodes from four mice per group. Data from multiple pooled experiments are denoted by different symbols within the same group. Graphs show mean \pm SD and were analyzed using unpaired Student's *t* test. *****P* < 0.0001; ****P* < 0.001; ***P* < 0.01; **P* < 0.05; *P* > 0.05 not significant (ns). BF = B cell follicles; TZ = T cell zone. Dashed lines represent T–B border. Figures A–I are representative of five independent experiments. Figures K and L are representative of three independent experiments.

approach. Large-scale macro-clustering could reflect a high precursor cell number after adoptive transfer. However, Th2 macro-clusters were also observed when examining endogenous polyclonal CD4 T cell responses after papain inoculation of 4get-GFP mice (Fig. S1 A). Moreover, large macro-clusters of IRF4, Gata3, and 4get-GFP-expressing endogenous polyclonal Th2 cells were detected after cutaneous infection with the helminth *Nippostrongylus brasiliensis* (*N.b.*) in skin-draining inguinal and gut-draining mesenteric LNs 3 and 6 days after infection, respectively, timepoints which reflect the tissue distribution of the parasite (Fig. S1, B and C) (von Moltke et al., 2016). Together, these data indicate that Th2 macro-clustering occurs in multiple type-II inducing conditions for both transferred monoclonal and endogenous polyclonal CD4 T cells.

As a comparison, we examined responses to OVA plus cytosine-phosphorothioate-guanine oligodeoxynucleotide (CpG) immunization, a TLR9 agonist that promotes Th1 differentiation (Leal et al., 2021). CpG OVA immunization elicited robust OT-II activation and proliferation indicated by Ki67 expression, but these T cells had undetectable Gata3 and 4get-GFP expression, corresponding to a lack of Th2 differentiation in these settings (Fig. 1 C). Of note, CpG also induced extensive Ki67 expression within B cell follicles, reflecting large-scale polyclonal B cell activation (Jiang et al., 2007). In contrast to papain responses, CpG immunization did not elicit the formation of dense T cell macro-clusters at the T–B border, but instead generated much smaller clusters which were more diffusely distributed throughout the T cell zone and the outer LN paracortex, consistent with past findings on behavior of CD4 T cells during Th1 differentiation (Fig. 1, C and D) (Groom et al., 2012; Leal et al., 2021).

Previous studies visualizing IL-4-producing cells in LNs at late time points have been conflated by the detection of IL-4-producing Tfh cells within B cell follicles (King and Mohrs, 2009; Prout et al., 2018), so we examined Tfh markers on the responding 4get-GFP⁺ T cells 2–3 days after papain OVA treatment. We found that most of the 4get-GFP⁺ cells displayed high levels of the high affinity IL-2 receptor, CD25, and low levels of CXCR5 and PD-1 staining (Fig. S1 D), indicating early effector T cell and not Tfh differentiation (Crotty, 2014; Johnston et al., 2012;

Ruterbusch et al., 2020). Similarly, endogenous activated (CD44⁺Ki67⁺) Gata3⁺ CD4 T cells expressed CD25 and lacked BCL6 expression, while a separate population of CD25⁻ cells coexpressed Gata3 and BCL6, indicating bifurcation of effector lineages (Fig. S1 E) (Chandler et al., 2022; Fang and Zhu, 2017; Johnston et al., 2009; Pepper et al., 2011). To verify that IL-4 mRNA competent 4get-GFP⁺ T cells also produced IL-4 protein, we examined responses in KN2^{+/-} reporter mice that express human CD2 (huCD2) on the surface of T cells actively producing IL-4 protein (Mohrs et al., 2005). We found abundant huCD2 expression on endogenous responding Gata3⁺ CD44⁺Ki67⁺ CD4 T cells, suggesting active IL-4 protein production (Fig. S1 F).

To investigate which specific myeloid cell population/s were associated with the Th2 macro-clusters, we next costained sections of papain-immunized auricular-draining LNs with various innate cell markers and used histocytometry and CytoMAP to analyze myeloid cell composition and distribution (Germer et al., 2012; Stoltzfus et al., 2020). Neighborhood clustering analysis identified distinct LN regions populated by different myeloid cell subsets (Fig. 1, E–I; and Fig. S1 G). As previously reported, migratory cDC2s, including CD301b⁺ (CD301b⁺MHC-II^{HI}) and Sirp⁺CD301b⁻ MHC-II^{HI} subsets, were predominantly localized in the outer T zone regions, with CD301b⁺ cDC2s localized at the T–B border and in close proximity to the edge of the Th2 macro-clusters (Fig. 1, E and F) (Kumamoto et al., 2013; León et al., 2012; Yi and Cyster, 2013). Of note, we observed relatively limited direct interdigitation of CD301b⁺ cDC2s within the inner regions of the macro-clusters, and instead, cDCs physically surrounded the proliferating Th2 cells (Fig. 1, E and F). In contrast to CD301b⁺ cDCs, CD207⁺MHC-II^{HI} DCs (Langerhans cells and migratory cDC1) were predominantly distributed within the deeper T cell zone and appeared spatially segregated from the Th2-dense regions (Fig. 1, E and F; and Fig. S1 G). Quantitative spatial distribution analysis across multiple LNs using CytoMAP confirmed these observations, demonstrating that CD301b⁺ cDC2s were the dominant myeloid cell subset preferentially enriched in Th2 macro-cluster tissue neighborhoods and that CD301b⁺ cDC2s and Th2 cells had a strong positive spatial correlation with one another (Fig. 1, G–I).

cDC2s have been previously demonstrated to drive Th2 polarization, but not T cell proliferation, after papain immunization (Allenspach et al., 2008; Castellanos et al., 2021; Kumamoto et al., 2013). To examine the requirement of migratory cDC2s for Th2 responses in our model, we examined OT-II cell responses in IRF4^{fl/fl} CD11c-Cre⁺ mice which exhibit impaired cDC2 activation and have reduced cDC2 migration from peripheral tissues into LNs, while keeping other cDC populations intact (Fig. S1, H–J) (Gao et al., 2013; Williams et al., 2013). Indeed, as compared with Cre⁻ littermate controls, loss of migratory cDC2 in Cre⁺ animals significantly reduced Gata3 and IRF4 expression in the responding OT-II cells without altering their clonal expansion (Fig. 1J). T cell macro-clustering was also significantly disrupted in Cre⁺ mice, together suggesting abrogated Th2 differentiation but not priming in the absence of migratory cDC2 (Fig. 1, K and L). cDC2s have also been reported to promote Tfh differentiation (Krishnaswamy et al., 2017; Li et al., 2016; Yin et al., 2021), and we noted reduced BCL6 expression in responding CD44⁺ Gata3⁻ OT-II cells in IRF4^{fl/fl} CD11c-Cre⁺ mice (Fig. 1J), suggesting that migratory cDC2s mediate the initiation of both Th2 and Tfh responses. Together, these data indicate that papain administration into the ear pinnae induces the formation of Th2-promoting microenvironments at the T–B border composed of macro-clusters of highly activated, early differentiating Th2 cells and CD301b⁺ migratory cDC2s driving Th2 response induction, and that this T cell clustering behavior is distinct from that seen during Th1 differentiation with TLR agonist immunization.

Th2 macro-clustering and differentiation are site-specific

Cutaneous exposure to allergens and associated antigens can occur in distinct anatomical locations. Surprisingly, when administering papain OVA into distinct skin sites, we observed major differences in Th2 response induction within the corresponding skin-draining LNs. As above, auricular LNs draining ear pinnae generated extensive early Th2 macro-clustering at the T–B border (Fig. 2A). In contrast, the equivalent dose of papain and OVA antigen administered in the footpad led to minimal Th2 differentiation in the draining brachial (Br) LNs (Fig. 2, B and C). Instead of macro-clustering at the T–B border, most OT-II cells in brachial LNs were more homogeneously distributed and localized in smaller clusters throughout the T cell zone and expressed significantly less Gata3 and 4get-GFP as detected by histo- and flow cytometry (Fig. 2, B–E). This was not due to a general lack of T cell activation, as following footpad immunization OT-II T cells in brachial LNs expressed abundant Ki67 and underwent equivalent or even greater levels of early proliferation as compared with those in auricular draining LNs (Fig. 2, B and E).

Site-specific differences between the ear and footpad were maintained for at least 6 days and across peripheral organs, with significantly reduced frequencies of effector Th2 OT-II cells found in the parenchyma of the lung and spleen, suggesting that divergent T cell responses were maintained even after OT-II cells migrated out of the original site of priming (Fig. 2, F and G). Despite the similar initial clonal bursts, by day 6, OT-II cells primed in auricular draining LNs exhibited increased expansion as compared with those primed in brachial LNs, and greater

numbers of OT-II cells disseminated to the spleen and lungs (Fig. 2G). At these later time points, the auricular draining LNs also exhibited increased frequency of CXCR5⁺PD-1⁺ Tfh OT-II cells, and the cells also expressed a greater amount of BCL6, suggesting that both Th2 and Tfh responses were linked to the specific skin site of immunization (Fig. S2A). Site-specific Th2 differences were also observed for endogenous CD4 T cells in KN2^{+/-} reporter mice, with a significant reduction of IL-4-producing Gata3⁺ CD4 T cells in footpad-draining brachial LNs (Fig. S2B). Endogenous Th2 response differences across immunization sites were also detected in Balb/c mice, indicating that this phenomenon was conserved across mouse strains with differential abilities to drive type-II immunity (Fig. S2C) (Hsieh et al., 1995).

We also examined whether site-specific Th2 differences occur after immunization with the adjuvant, Alum, which has no known protease activity. As above, Alum plus OVA immunization of the ear pinnae elicited robust OT-II macro-clustering and Th2 differentiation in auricular draining LNs, but this was markedly reduced in brachial LNs after footpad administration (Fig. 2, H and I; and Fig. S2, D and E). Differences in Th2 responses across the sites were also detected in endogenous polyclonal CD4 T cells after Alum immunization (Fig. S2D). We next examined Th1 differentiation settings after CpG OVA immunization. In stark contrast to type-II inflammation settings, CpG OVA resulted in equivalent expansion, T-box transcription factor (Tbet) expression, and CXCR3 expression in responding OT-II cells in both auricular and brachial LNs, indicating comparable Th1 response formation between the different cutaneous sites (Fig. 2E). Equivalent Th1 responses across these distinct LNs were also previously observed with other type-I adjuvants (Leal et al., 2021), together suggesting that site-specific Th2 induction differences do not necessarily extend to other helper cell lineages, such as Th1 responses.

Given these findings, we hypothesized that non-equivalent Th2 responses in different skin-draining LNs could result from either intrinsic differences between the LNs, differential lymphatic drainage of antigens and agonists, or fundamental differences in how distinct cutaneous sites program local immune responses. To investigate whether brachial LNs have an inherent defect in mounting Th2 immunity, we immunized mice with papain OVA in the dorsal skin of the flank, which targets a different skin dermatome, but with antigen and agonist also draining into brachial LNs. Although generating more heterogeneous responses as compared with footpad inoculation, likely due to more diffuse agonist dispersal across the subcutaneous tissue compartment, flank injection resulted in Th2 induction in brachial LNs, which was more analogous to that found in auricular LNs with ear immunization (Fig. S2, F and G). We also tested other cutaneous sites, including the hind paw and the tail base which drain the popliteal and inguinal LNs, respectively. Similar to brachial LN responses with forepaw injection, hind paw inoculation also elicited limited Th2 responses in the draining popliteal LNs, with decreased Gata3 expression by activated OT-II cells. In contrast, tail base administration of papain OVA generated heightened Th2 responses within the inguinal draining LNs (Fig. S2, F and G). We next examined whether site-

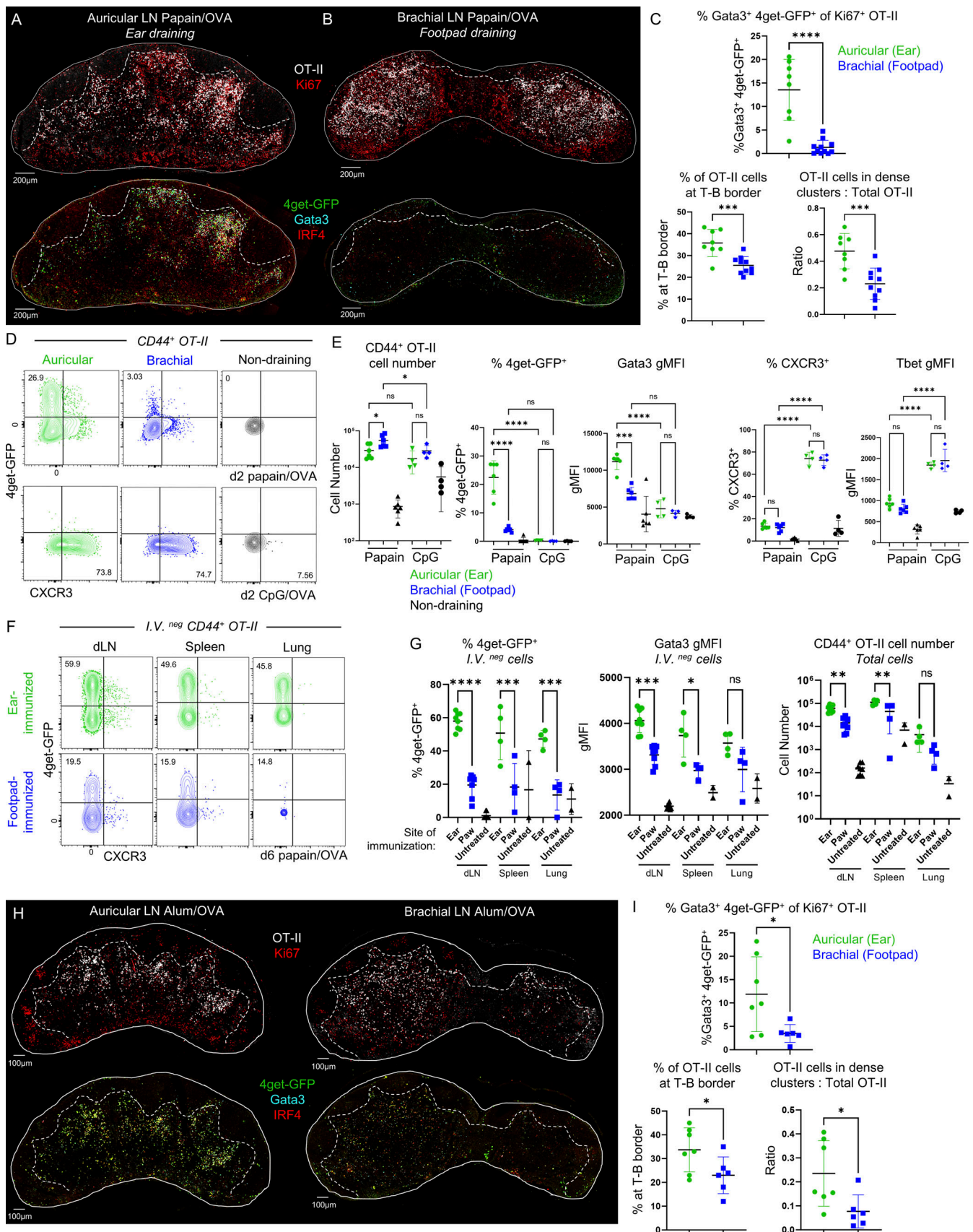


Figure 2. **Th2 macro-clustering and differentiation are site-specific.** (A–E) Mice were transferred with naive 4get.OT-II cells as in Fig. 1A, injected with the indicated adjuvant plus OVA at different sites in the ear pinnae or front footpad, and corresponding dLNs were harvested and assessed by histocytometry and

flow cytometry at 48 h. Representative images depicting OT-II macro-clustering and Th2 differentiation at the T–B border in (A) auricular versus (B) brachial dLNs. (C) Histocytometry analysis of the percent activated OT-II coexpressing 4get-GFP and Gata3, OT-II localization, and the ratio of macro-clustered versus total OT-II in the indicated LNs. (D and E) Representative flow plots and quantification of CD44⁺ OT-II cell number, frequency of 4get-GFP⁺ and CXCR3⁺ cells, and Gata3 and Tbet gMFI of CD44⁺ OT-II cells. (F and G) 0.5×10^6 naive 4get.OT-II cells were transferred to recipients and then injected with papain OVA in the ear pinnae or front footpad. 6 days later, cells were labeled intravenously, and dLNs, spleen, and lung were harvested and assessed by flow cytometry. Representative plots and quantification of frequency of 4get-GFP⁺ and Gata3 gMFI of IV⁻ CD44⁺ OT-II cells and total CD44⁺ OT-II cell number are shown. (H and I) Mice were treated as in A but were immunized in the ear pinnae and front footpad with Alum plus OVA. (H) Representative images depicting OT-II macro-clustering and Th2 differentiation at the T–B border in auricular versus brachial dLNs. (I) Histocytometry analysis of the percent activated OT-II coexpressing 4get-GFP and Gata3, OT-II localization, and the ratio of macro-clustered versus total OT-II in the indicated LNs. Data shown represent one independent experiment with at least $n = 4$ independently immunized lymph nodes from two mice per group. Graphs show mean \pm SD and were analyzed using unpaired Student's *t* test. *****P* < 0.0001; ****P* < 0.001; ***P* < 0.01; **P* < 0.05; *P* > 0.05 not significant (ns). Au = auricular; Br = brachial; IV = intravenous. Dashed lines represent T–B border. A–E are representative of five independent experiments; F–I are representative of two independent experiments.

specific Th2 response differences would be maintained in a model that does not involve abundant lymphatic drainage induced by injection. To test this, we painted the ear versus front footpad skin with dibutyl phthalate (DBP) to induce Th2-driven contact hypersensitivity in which antigen and adjuvant are administered epicutaneously and not intradermally (Larson et al., 2010). Although DBP painting did not induce as potent proliferative responses as papain injection, major differences in Th2 differentiation were still observed across the draining LNs, with markedly increased Gata3 and IRF4 expression in responding CD4 T cells within auricular but not brachial draining LNs (Fig. S2 H). Together, these findings indicate that distinct cutaneous sites have non-equivalent abilities to drive Th2 macro-clustering and Th2 differentiation and that this does not simply result from intrinsic differences between the lymphoid organs or is restricted to injection- or protease-based models, indicating a more generalizable divergence in the ability of distinct skin sites to drive Th2 responses.

Costimulatory molecule expression is enhanced on migratory cDC2s derived from auricular LNs

Given the critical role of cDC2s in driving Th2 responses, we next examined the hypothesis that migratory cDC2 responses were non-equivalent between the distinct dermal tissue responses. To test this, we immunized mice with papain plus the fluorescent protein EαGFP into the forepaw or ear pinnae (Itano et al., 2003) and examined antigen-bearing migratory DCs in the corresponding draining LNs. Albeit some variation was observed among individual samples across multiple experiments, we found no major differences in the number of total cDC2s, antigen-bearing EαGFP⁺ cDC2s, or the amount of EαGFP captured by these cells between the sites (Fig. 3, A–C; and Fig. S3 A). The dominant antigen-bearing population in both draining LNs were the CD301b⁺ cDCs (Fig. S3 B) and their total number did not differ between draining LNs (Fig. 3 C). The overall composition of antigen-bearing myeloid cells was also largely similar across the LNs, albeit a modest increase in the frequency of antigen-bearing CD301b⁺ DCs and CD64⁺ cells and a corresponding decrease in CD301b⁻CD11b⁻ DCs in brachial LNs was noted (Fig. S3 B).

We also examined the amount of pMHC-II complex on the DC surface using the Y-Ae antibody, which recognizes the Eα peptide presented on I-Ab (Itano et al., 2003). Surprisingly, we found that while papain induced robust antigen uptake by migratory cDCs, it was not associated with detectable pMHC-II

complex on the cell surface (Fig. S3, C and D). Minor differences in the total number, but not frequency, of EαGFP⁺ Y-Ae⁺ migratory DCs were noted between auricular and brachial LNs after papain immunization (Fig. S3 D). In contrast to papain settings, EαGFP plus CpG immunization elicited both antigen uptake and robust surface pMHC-II expression by migratory cDCs (Fig. S3, C and D), demonstrating major differences in how type-I and type-II stimuli impact MHC-II antigen processing and presentation and suggesting that during *in vivo* type-II responses to papain, surface pMHC-II expression is relatively limited on migratory cDCs. Of note, Eα peptide sequence analysis did not identify papain cleavage sites, indicating that the divergence in pMHC-II complex between papain and CpG conditions was not simply a result of protease-mediated degradation of the Eα peptide.

To further interrogate potential differences among migratory cDCs from different cutaneous sources, we next sorted antigen-bearing (EαGFP⁺) migratory cDC2 subsets (MHC2^{HI}CD11c^{Int}CD301b^{+/-}CD11b^{+/-}) from auricular and brachial draining LNs 2 days post papain plus EαGFP immunization, or from naïve mice, and performed bulk RNA sequencing. As expected, principal component analysis (PCA) of all samples demonstrated that the primary segregation was driven by the immunization state, with samples clustering based on whether they were obtained from naïve or papain-immunized LNs, revealing large-scale transcriptional changes across all cDC populations from both tissues after papain immunization (Fig. 3 D, left; Fig. S3, E and F). Of note, IL-12b, which is constitutively expressed by migratory cDCs at a steady state (Conejero et al., 2017; Everts et al., 2016), was downregulated upon papain immunization (Fig. S3 F). When considering only the papain immunized samples, further PCA separation demonstrated that sample divergence on the PCA1 axis was dominantly driven based on the specific LN of origin, indicating major transcriptional differences between the antigen-bearing auricular-derived and brachial-derived cDCs, while also maintaining a secondary level grouping along the PCA2 axis based on the cell subset (Fig. 3 D, right; Fig. S3 E). Of the top 100 differentially expressed genes (DEGs) between sites, DCs from auricular LNs preferentially upregulated genes associated with activation and costimulation including *Cd80*, *Cd86*, *Cd274* (PDL1), and *Pcdllg2* (PDL2), indicating increased cDC2 maturation (Fig. 3, E and F). Divergent expression of these molecules at the protein level was confirmed by flow cytometry, demonstrating that antigen-bearing migratory cDC2s in

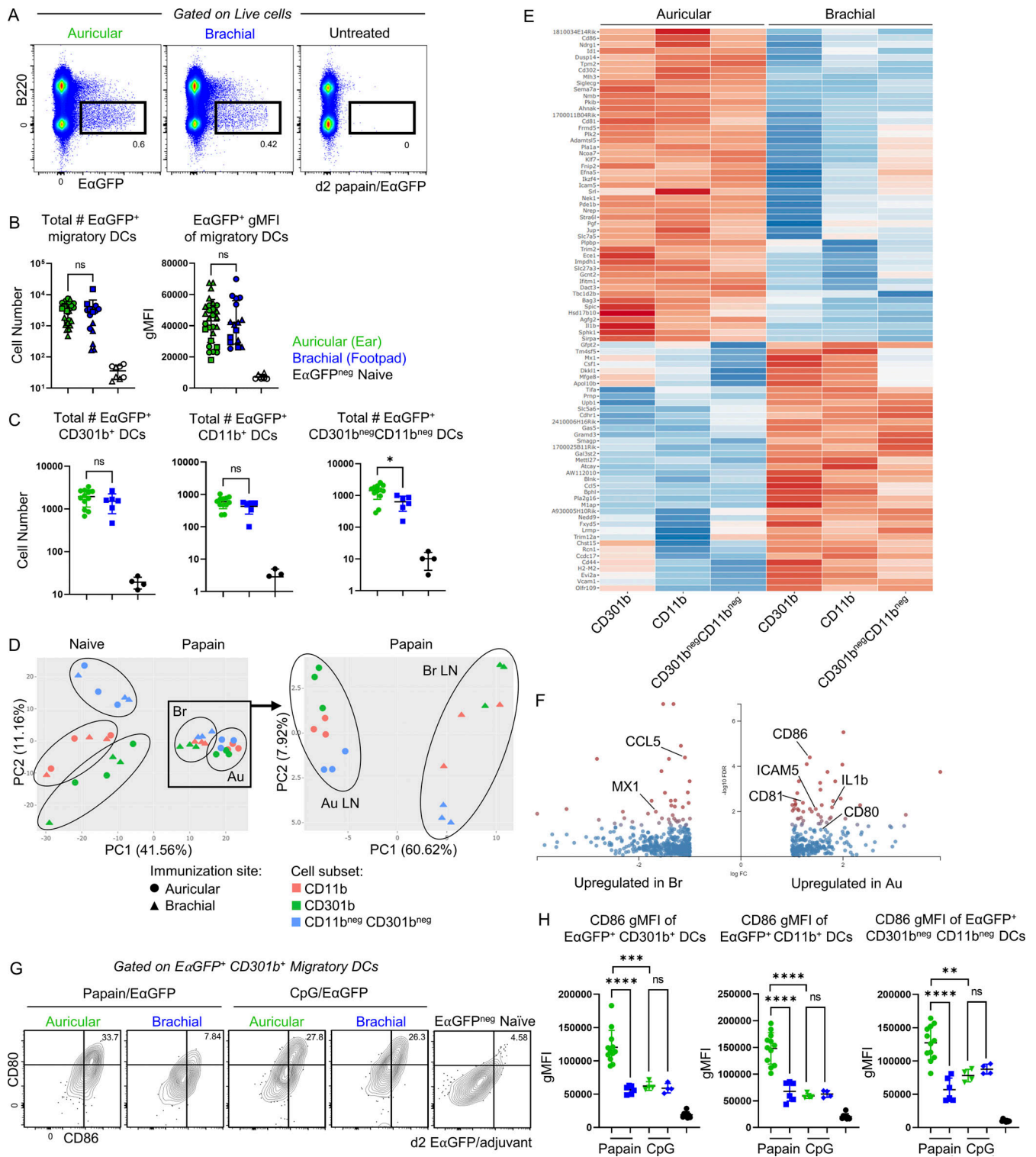


Figure 3. Transcriptional signatures of migratory DCs in distinct draining LNs. B6 mice were immunized in the ear pinnae and front footpad with papain plus EαGFP and the corresponding dLNs were harvested 48 h later. **(A)** Representative plots showing total EαGFP expression within live cells. **(B)** Quantification of the number of EαGFP⁺ migratory DCs and EαGFP⁺ gMFI of migratory DCs. **(C)** Quantification of total EαGFP⁺ cells for the indicated DC subsets. **(D–F)** EαGFP⁺ DC populations were sorted from dLNs on day 2 for bulk RNA sequencing. DCs were sorted on Live, CD64⁻, Lineage⁻ (CD3, CD19, NK1.1), EαGFP⁺, MHC-II^{hi} CD11c^{int}, XCR1⁻, EpCAM⁻, then sorted into CD11b⁺ CD301b⁺, CD11b⁺ CD301b⁻, and CD11b⁻ CD301b⁻ populations. The same gates were used for EαGFP⁻ DCs in naïve LNs. **(D)** PCA plot of all samples (left) and papain immunized DC populations (right). **(E)** Heatmap of the top 100 DEGs between EαGFP⁺ migratory DCs from auricular versus brachial dLNs (FDR < 0.05, 2× fold change expression). **(F)** Volcano plot of DEGs between antigen-bearing migratory DCs from auricular versus brachial dLNs. Red indicates a FDR < 0.05. Genes with a log fold change > 2 are shown. **(G and H)** EαGFP⁺ migratory DCs were assessed for surface CD80 and CD86 expression by flow cytometry. **(G)** Representative flow plots for CD80 and CD86 expression on EαGFP⁺ CD301b⁺ cDC2s after papain OVA or CpG OVA immunization and **(H)** quantification for three indicated DC subsets are shown. Data shown represents one independent

experiment with at least $n = 4$ independently immunized lymph nodes from two mice per group. Data from multiple pooled experiments are denoted by different symbols within the same group. Graphs show mean \pm SD and were analyzed using unpaired Student's t test. **** $P < 0.0001$; *** $P < 0.001$; ** $P < 0.01$; * $P < 0.05$; $P > 0.05$ not significant (ns). A–C, G, and H are representative of three to four independent experiments. D–F are representative of one independent RNA sequencing experiment with $n = 3$ per group.

auricular LNs expressed significantly higher levels of CD80 and CD86 costimulatory molecules as compared with their antigen-bearing counterparts from brachial LNs (Fig. 3, G and H; and Fig. S3 G). In contrast to papain administration, CpG immunization of different cutaneous sites elicited comparable expression of CD80 and CD86 on migratory cDCs, again highlighting the divergence of how type-I versus type-II inflammation impacts the immune response (Fig. 3, G and H). In addition to costimulatory molecule differences after papain exposure, several cDC2 subsets in brachial LNs expressed gene signatures enriched in type 1 interferon (IFN) and viral sensing pathways, such as the interferon-stimulated gene, *Mxl*, while gene signatures in auricular LN cDC2s were enriched in cytokine-mediated and leukocyte proliferation signaling pathways, together demonstrating additional differences between the sites (Fig. 3 F and Fig. S3 H). Together, these data suggest that while being relatively similar prior to inflammation, cDC2s migrating into LNs from different cutaneous tissues exhibit marked differences at the transcriptional and protein levels, in particular for costimulatory molecule expression.

Site-specific T cell response differences are mediated through non-equivalent expression of costimulatory molecules by migratory cDCs

Costimulation synergizes with TCR signaling to drive optimized T cell activation and has been implicated in Th2 differentiation (Acuto and Michel, 2003; Bhattacharyya and Feng, 2020; Chen and Flies, 2013; Gause et al., 1997; King et al., 1995; Rulifson et al., 1997; Tao et al., 1997; van Rijt et al., 2004). Given the costimulatory molecule expression differences on DCs between the sites, we investigated whether signaling pathways downstream of TCR and costimulation were also nonequivalent in activated T cells in different draining LNs. Indeed, we found significantly higher expression of the AP-1 transcription factors, basic leucine zipper transcription factor (BATF) and IRF4, in activated OT-II T cells within the ear-draining auricular LNs, indicating non-equivalent engagement of the TCR/costimulatory molecule signaling platform (Fig. 4, A and B; and Fig. 2, A and B). Expression of the transcription factors BATF and IRF4 in T cells has been previously associated with Th2 differentiation and IL-4 production (Bao et al., 2016; Huber and Lohoff, 2014; Iwata et al., 2017; Krishnamoorthy et al., 2017; Kuwahara et al., 2016; Li et al., 2012; Lohoff et al., 2002; Rengarajan et al., 2002; Sahoo et al., 2015), and we observed a strong positive correlation of these molecules with each other and Gata3 and 4get-GFP expression (Fig. 4 C). Image-based analysis also demonstrated increased phosphorylation of the mTOR signaling protein S6 (pS6), also downstream of TCR/costimulation platform, in T cells within auricular draining LNs (Fig. 4 D). Unexpectedly, in contrast to type-II inflammation, CpG OVA promoted overall reduced levels of pS6 and IRF4 as compared with papain within auricular LNs, and equivalent site-specific

expression across both LN sites (Fig. 4, A and D). This indicates that Th2 differentiation is associated with relatively enhanced and not reduced T cell activation, and that site specificity in T cell response induction does not extend to all T helper cell lineages.

Together, these findings suggested that after papain immunization, CD4 T cells within ear-draining auricular LNs experienced increased overall stimulation compared with forepaw-draining brachial LNs. While being consistent with differential expression of costimulatory molecules by migratory cDC2s (Fig. 3, G and H) and with otherwise limited differences in the number and composition of antigen-bearing migratory cDCs across the sites, it was still possible that insufficient delivery of antigen to brachial LNs after paw immunization was mediating the reduced T cell activation and Th2 programming in this compartment. To test this possibility, we titrated the amount of OVA administered into the skin sites along with a fixed concentration of papain. Although increasing the OVA dose at each site up to 10 \times the original amount increased OT-II clonal expansion in both draining LNs, this did not result in enhanced Th2 responses in brachial LNs, suggesting that the total amount of antigen was not a limiting factor in driving reduced Th2 differentiation after footpad immunization (Fig. 4 E). Of note, increased antigen delivery also did not elicit increased Tbet expression in responding T cells, indicating that high antigen dose availability does not necessarily promote Th1 skewing in papain immunization settings (Fig. 4 E).

Based on the above observations, we next directly tested the requirements for costimulatory molecule expression on Th2 differentiation in vivo. For this, we performed a timed blockade of costimulatory signaling by administering an anti-CD28 antibody 24 h after immunization and harvesting LNs 24 h later. Delayed anti-CD28 administration allows the T cells to mount initial cognate interactions with cDCs for early priming and activation, but limits the prolonged costimulatory contacts during the differentiation phase (Mempel et al., 2004). Indeed, delayed CD28 blockade resulted in very modest reductions of OT-II cellularity, indicating relatively normal initial activation (Fig. 5 A), but markedly decreased the expression of 4get-GFP, Gata3, BATF, and pS6 in both auricular and brachial LNs (Fig. 5, A–C). Delayed CD28 blockade also resulted in reduced macrocluster formation within auricular LNs, instead driving more homogeneous and non-clustered distribution of OT-II cells throughout the T zone, akin to responses observed in footpad draining brachial LNs (Fig. 5, B and D). Furthermore, delayed CD28 blockade also reduced endogenous polyclonal Th2 cell differentiation, suggesting these effects are mediated across an array of TCR affinities (Fig. S4 A). Given that costimulation is thought to promote general T cell activation for all helper cell lineages, we next tested whether prolonged costimulatory sensing was important in Th1-inducing settings after CpG OVA immunization. Delayed CD28 blockade elicited much more

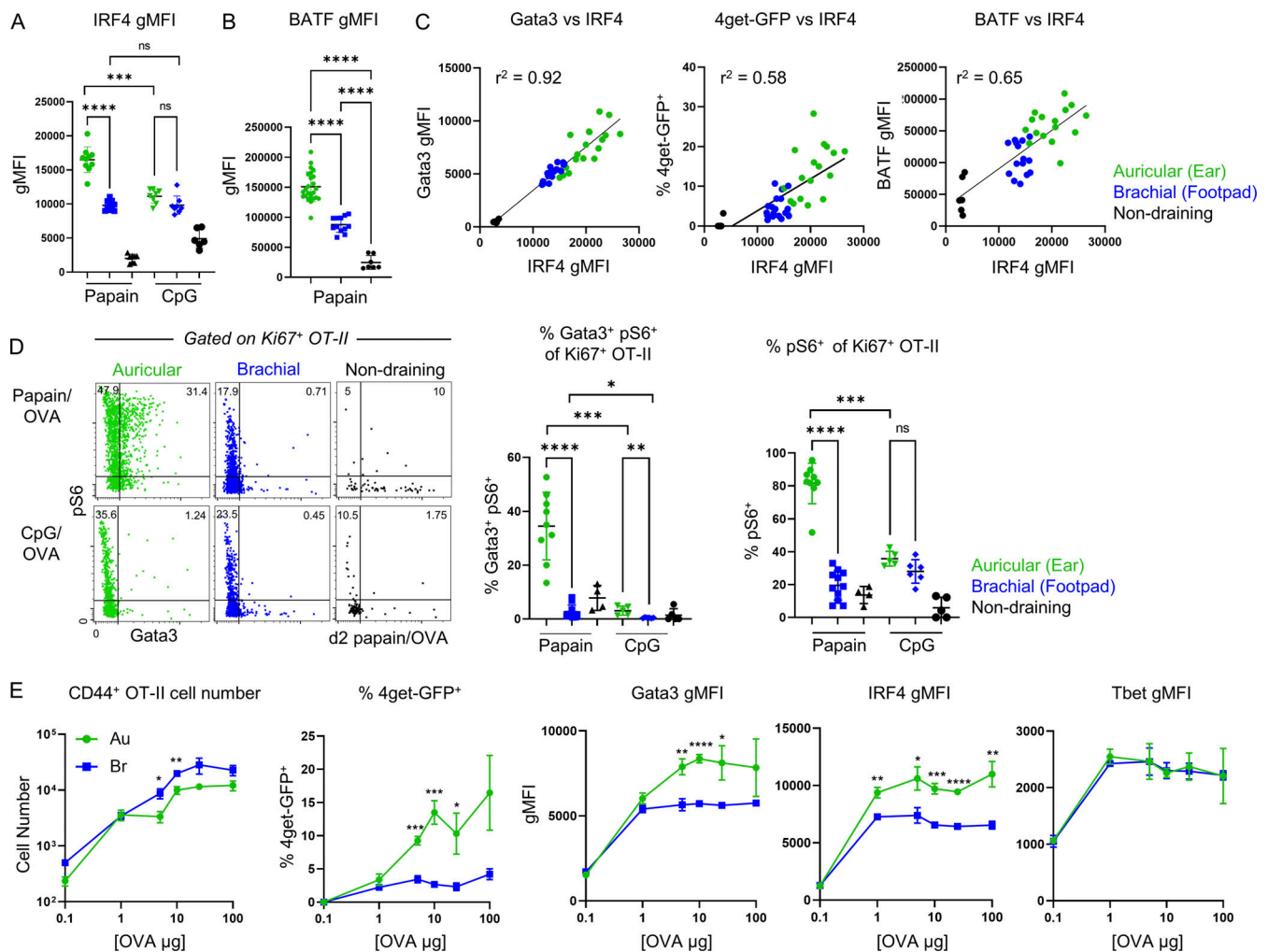


Figure 4. Non-equivalent activation of T cells across skin-draining LNs. (A–D) Mice were transferred with naïve 4get.OT-II cells, injected with papain OVA or CpG OVA in the ear pinnae or front footpad, and dLNs were harvested and assessed by histocytometry or flow cytometry at 48 h. **(A and B)** Expression of IRF4 and BATF on CD44⁺ OT-II cells after immunization with the indicated adjuvant. **(C)** Correlation plots of IRF4 gMFI with Gata3 gMFI, BATF gMFI, and frequency of 4get-GFP⁺ cells across different dLNs are shown. **(D)** Representative histocytometry plots and quantification of the frequency of pS6 and Gata3 expression in IRF4⁺Ki67⁺ OT-II T cells. **(E)** Mice transferred with naïve 4get.OT-II cells were injected with a fixed amount of papain and an increasing amount of OVA, as indicated, in the ear pinnae or front footpad then dLNs were harvested and assessed by flow cytometry at 48 h. CD44⁺ OT-II cell number, frequency of 4get-GFP⁺ cells, and Gata3, IRF4, and Tbet gMFI expression on CD44⁺ OT-II cells are shown. Data shown represents one independent experiment with at least $n = 4$ independently immunized lymph nodes from two mice per group. Graphs show mean \pm SD and were analyzed using unpaired Student's *t* test. **** $P < 0.0001$; *** $P < 0.001$; ** $P < 0.01$; * $P < 0.05$; $P > 0.05$ not significant (ns). All figures are representative of at least three independent experiments.

modest effects on CXCR3 and Tbet expression (Fig. S4 B), overall indicating that prolonged costimulation was less essential in Th1-inducing settings.

To examine if increasing costimulation can directly modulate Gata3 expression and Th2 differentiation in vitro, we next cultured naïve OT-II T cells in non-polarizing culture conditions with varying concentrations of plate-bound anti-CD3 and anti-CD28 for 48 h. We found that increasing the concentration of available CD28 significantly enhanced Gata3 expression in T cells, and this was particularly evident at low anti-CD3 concentrations (Fig. 5, E–G). IRF4 was also increased in a CD28-dependent manner, indicating that this transcription factor can be regulated by both TCR and costimulation (Fig. 5, E and F). Additional blockade of IFN- γ further increased Gata3 expression across both low and intermediate anti-CD3 culture conditions,

supporting its role in suppressing Th2 cell differentiation (Fig. 5, F and G). Moreover, dose-dependent CD28-mediated effects on Gata3 expression were observed in Th2-polarizing culture conditions, albeit Gata3 and IRF4 expression was significantly greater than in non-polarizing settings (Fig. S4 C). Together, these data suggest that costimulation can directly enhance T cell activation and Th2 differentiation by inducing IRF4 and Gata3 expression and that differences in differentiation across the distinct skin-draining LNs are most likely driven by non-equivalent expression of costimulatory molecules by migratory cDC2s.

Th2 macro-clustering and differentiation is LFA-1 dependent

The above findings indicated that prolonged costimulatory molecule availability from migratory cDC2s promotes T cell macro-clustering and Th2 differentiation (Fig. 5 B), and we next

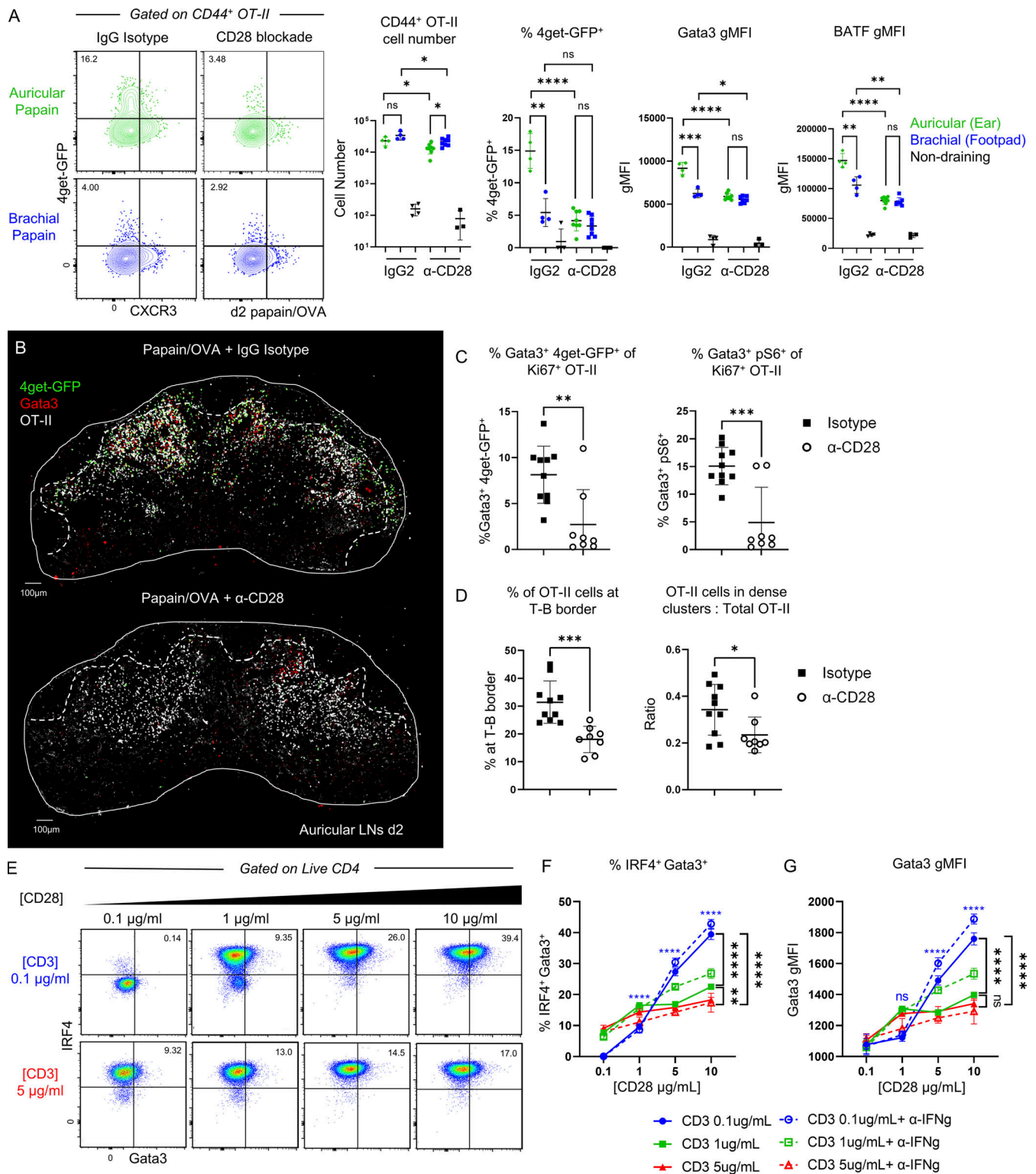


Figure 5. Site-specific T cell responses are mediated through non-equivalent expression of costimulatory molecules by migratory cDCs. (A–D) Mice were transferred with naïve 4get.OT-II cells, treated with papain OVA as in Fig. 1 A, and administered α-CD28 blocking antibody or IgG isotype control intraperitoneally 24 h post immunization and dLNs were harvested and assessed by histocytometry or flow cytometry at 48 h. **(A)** Representative flow plots and quantification of CD44⁺ OT-II cell number, 4get-GFP⁺ frequency, and Gata3 and IRF4 gMFI of CD44⁺ OT-II cells after α-CD28 or isotype control treatment. **(B)** Representative images depicting OT-II macro-clustering and Th2 differentiation in auricular dLNs treated with isotype control (top) or α-CD28 blocking antibody (bottom). **(C and D)** Histocytometry analysis of 4get-GFP, Gata3, and pS6 expression, OT-II localization at the T–B border, and ratio of densely clustered Ki67⁺ OT-II cells with the indicated treatment. **(E–G)** Naïve OT-II cells were cultured in vitro with the indicated concentrations of α-CD3 and α-CD28. α-IFNγ was added to cultures in some conditions (dashed lines). Cells were harvested 48 h later and assessed for expression of Gata3 and IRF4 by flow cytometry. Data shown represents one independent experiment with at least *n* = 4 independently immunized lymph nodes from two mice per group or three

wells per treatment group. Graphs show mean \pm SD and were analyzed using unpaired Student's *t* test. *****P* < 0.0001; ****P* < 0.001; ***P* < 0.01; **P* < 0.05; *P* > 0.05 not significant (ns). Dashed lines represent T-B border. A–D are representative of at least two independent experiments. E–G are representative of four independent experiments.

examined the mechanisms driving prolonged T cell–DC interactions. The integrin lymphocyte function-associated antigen 1 (LFA-1) is rapidly upregulated on T cells following activation, and its ligand, intercellular adhesion molecule 1 (ICAM-1), is expressed on DCs after maturation to mediate T cell–DC interactions (Gérard et al., 2013, 2021). LFA-1 has also been shown to reduce the threshold of TCR/costimulatory signaling required for T cell activation, thus enabling increased activation in the setting of low pMHC-II (Wang et al., 2008). We observed marked ICAM-1 upregulation on activated antigen-bearing E α GFP⁺ migratory DCs in both brachial and auricular LNs as compared with non-antigen-bearing E α GFP⁻ migratory DCs (Fig. 6 A). Of note, ICAM-1 was upregulated to a greater degree after papain as compared with CpG immunization, suggesting a divergence in DC activation states during type-I versus type-II inflammation settings (Fig. 6 A).

To test if T cell macro-clustering and Th2 differentiation were driven by prolonged LFA-1 dependent cellular interactions, we performed a delayed integrin blockade, treating mice with an anti-LFA-1 blocking antibody 24 h post papain OVA administration and examining responses in auricular and brachial LNs 24 h later (Gérard et al., 2013; Krummel et al., 2018). Delayed LFA-1 blockade did not markedly alter OT-II T cell proliferation, indicating relatively normal initial activation (Fig. 6, B and C). In contrast, 4get-GFP, Gata3, and IRF4 expression were significantly decreased with LFA-1 blockade, indicating reduced Th2 differentiation (Fig. 6, B, C, and E). LFA-1 blockade also disrupted the T cell macro-clustering at the T-B border, indicating the limited formation of Th2 microenvironments (Fig. 6, D and E). In addition, delayed LFA-1 blockade reduced the generation of endogenous Th2 responses, indicating that this pathway is important for T cells with diverse TCR affinities (Fig. S5 A). We also performed the delayed LFA-1 blockade during *N.b.* helminth infection. To account for the heterogeneity of infection and T cell responses, mice were treated with LFA-1 blocking antibody on days 2 and 3 after infection, and the draining inguinal LNs were harvested on day 4. We found that delayed LFA-1 blockade significantly reduced Gata3 expression in responding Ki67⁺ T cells, as well as minimized Th2 macro-clustering (Fig. 6, F and G), together indicating that prolonged LFA-1 integrin-mediated interactions are important for Th2 responses in diverse type-II inflammation settings. In contrast to type-II stimuli, delayed LFA-1 blockade had a minimal effect on Th1 differentiation after CpG OVA immunization (Fig. S5, B and C).

After activation, T cells can also express ICAM-1 on the cell surface, and in addition T–DC interactions could potentially engage in homotypic T–T cell contacts (Gérard et al., 2013). To dissect whether delayed LFA-1 blockade was primarily affecting T–DC or T–T cell interactions, we next generated ICAM1.KO OT-II cells (Fig. S5 D) and compared these responses with WT OT-II cells. In these experimental settings, ICAM1.KO OT-II T cells retain normal LFA-1 integrin functionality and can interact with

ICAM1-expressing cDCs but lack the ability to engage in homotypic T–T cell contacts. We found no defects in Th2 differentiation in ICAM-1 deficient OT-II T cells, indicating that LFA-1/ICAM-1 mediated homotypic T–T interactions are not required for early Th2 responses (Fig. S5 E). Together, these data suggest that enhanced T cell activation via costimulatory molecule expression by cDCs promotes prolonged LFA1 integrin-mediated T–DC interactions within auricular ear-draining LNs. These contacts in turn drive the formation of T cell macro-clusters and promote Th2 differentiation.

Increased costimulation promotes enhanced cytokine signaling and Th2 differentiation

Costimulation stimulates the production of IL-2 by activated T cells, as well as can elicit the production of the Th2 cytokine IL-4 in vitro (Acuto and Michel, 2003; Bhattacharyya and Feng, 2020; Chen and Flies, 2013; Gause et al., 1997; King et al., 1995; Rulifson et al., 1997; Tao et al., 1997; van Rijjt et al., 2004). IL-2 signaling in turn increases expression of the IL-4 receptor, IL-4R α , such that IL-2-stimulated T cells become more receptive to IL-4 (Liao et al., 2008). T cell costimulation and macro-clustering could thus promote increased local bioavailability of the cytokines, IL-2 and IL-4, produced directly by activated T cells, and these could reinforce localized Th2 differentiation. Indeed, we found CD25 was highly expressed on the activated CD44⁺ Gata3⁺ OT-II Th2 cells (Fig. 7 A). Further, early Gata3⁺CD25⁺ Th2 cells had increased expression of phosphorylated (p)STAT5 and pSTAT6, indicating enhanced and/or sustained IL-2 and IL-4 signaling, respectively, as compared with Gata3⁻CD25⁻ non-Th2 cells (Fig. 7 B).

Consistent with non-equivalent T cell activation and differentiation in different draining LNs, both pSTAT5 and pSTAT6 in responding OT-II cells were significantly elevated in auricular as compared with brachial draining LNs (Fig. 7 C). pSTAT levels were also directly correlated with non-equivalent Gata3 expression across the sites (Fig. 7 D), suggesting direct involvement in Th2 differentiation. We thus tested whether differential costimulatory molecule engagement by responding T cells in distinct LNs resulted in non-equivalent cytokine signaling and Th2 differentiation. For this, we again used the timed CD28 blockade and examined the phosphorylation of STAT5 and STAT6 molecules 24 h later. We found that delayed anti-CD28 treatment significantly reduced pSTAT5 and pSTAT6 expression in auricular draining LNs, and abrogated the differences between the tissues (Fig. 7, E and F). Similar effects were observed after in vivo anti-IL-2 blockade, and both anti-CD28 and anti-IL-2 treatments resulted in comparable decreases in STAT5, and to a lesser extent STAT6, phosphorylation (Fig. 7, E and F). Both anti-CD28 and IL-2 blockade markedly reduced Gata3 expression in responding OT-II cells, indicating a clear link between prolonged costimulation, cytokine sensing, and Th2 differentiation (Fig. 7 F). Finally, we tested whether cytokine signaling

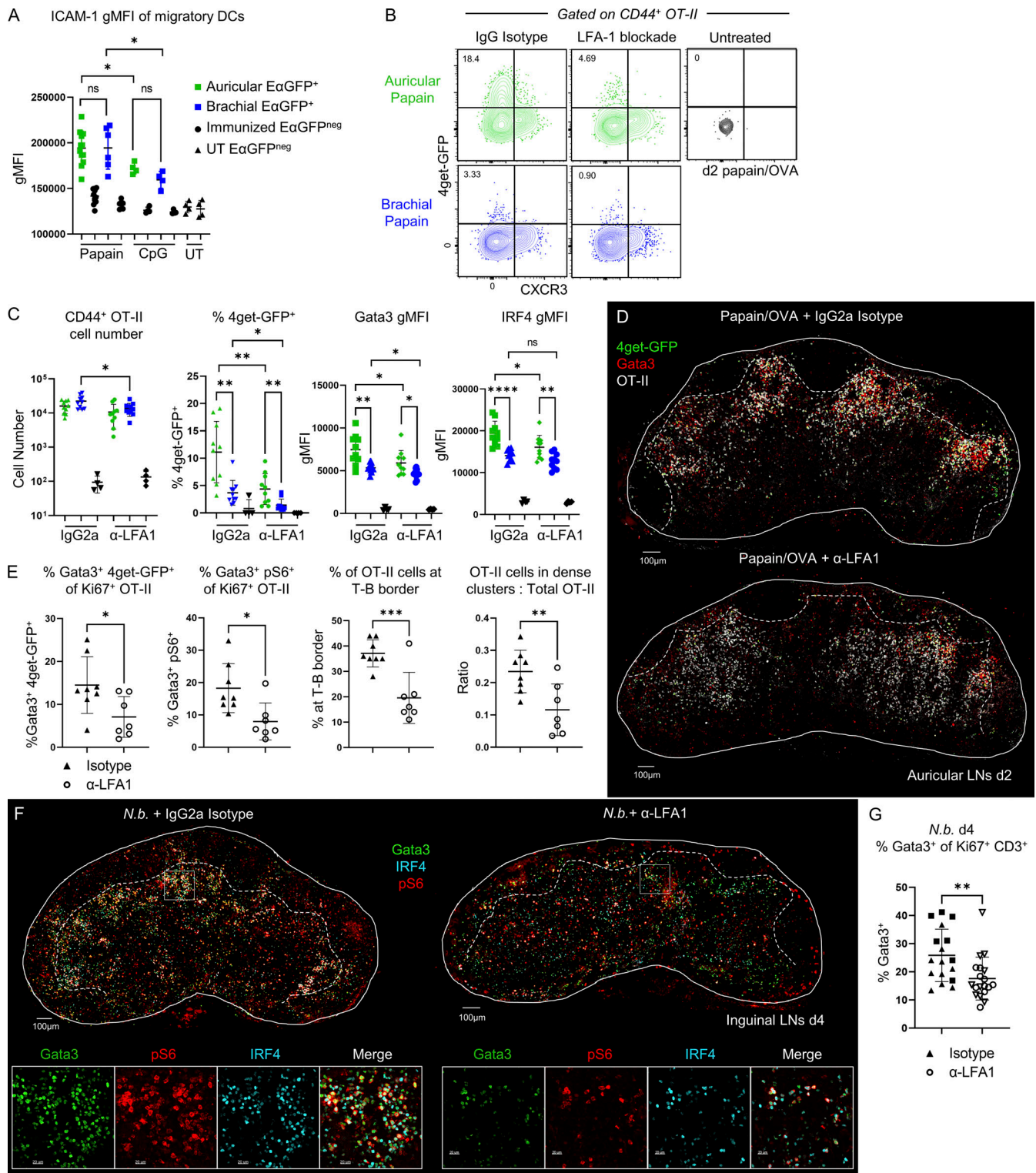


Figure 6. Th2 macro-clustering and differentiation is LFA-1 dependent. (A) B6 mice were immunized in the ear pinnae and front footpad with papain or CpG plus E α GFP and harvested for flow cytometry 48 h later. Expression of ICAM-1 on E α GFP⁺ and E α GFP⁻ or naive (untreated, UT) migratory DCs in the indicated LNs is shown. (B–E) Mice were transferred with naive 4get.OT-II cells, treated with papain OVA as in Fig. 1 A, and administered α -LFA1 blocking antibody or IgG isotype control intraperitoneally 24 h after immunization and dLNs were harvested and assessed by histocytometry or flow cytometry at 48 h. (B) Representative flow plots and (C) quantification of the number of CD44⁺ OT-II cells, frequency of 4get-GFP⁺ cells, and Gata3 and IRF4 gMFI of CD44⁺ OT-II cells with the indicated treatment. (D) Representative images depicting OT-II macro-clustering and Th2 differentiation in auricular dLN treated with isotype control (top) or α -LFA-1 blocking antibody (bottom). (E) Histocytometry analysis of 4get-GFP, Gata3, and pS6 expression, OT-II localization at the T–B border, and the ratio of densely clustered OT-II cells with the indicated treatment is shown. (F and G) B6 mice were inoculated subcutaneously at the tail base with 500 N.b. L3 larvae, treated intraperitoneally with α -LFA1 blocking antibody or IgG isotype control on day 2 and 3 after infection, and the inguinal dLNs, or LNs

from naive mice, were harvested on day 4 for confocal microscopy. **(F)** Representative images and zoom-ins depicting Th2 macro-clustering with α -LFA1 blocking antibody or isotype control. Gata3 signal is masked outside of Ki67⁺ activated cells for visual clarity. **(G)** Histocytometry analysis of Gata3 expression in Ki67⁺ T cells with the indicated treatment. Data shown represent one independent experiment with at least $n = 8$ independently immunized lymph nodes from four mice per group. Data from multiple pooled experiments are denoted by different symbols within the same group. Graphs show mean \pm SD and were analyzed using unpaired Student's *t* test. Paired *t* tests were performed when comparing responses within the same experimental tissue (panel A). **** $P < 0.0001$; *** $P < 0.001$; ** $P < 0.01$; * $P < 0.05$; $P > 0.05$ not significant (ns). Dashed lines represent T-B border. A-C are representative of four independent experiments. D-G are representative of two independent experiments.

was upstream or downstream of costimulatory molecule sensing and macro-cluster formation. We found that delayed administration of IL-2 blocking antibody did not alter T cell macro-clustering, but significantly reduced Gata3 and 4get-GFP expression in responding OT-II cells (Fig. 7, G and H). These results indicate that increased sensing of costimulatory molecules by early differentiating T cells in ear-draining auricular LNs is associated with enhanced T cell macro-clustering, increased local IL-2 and IL-4 cytokine production and sensing, and these together lead to amplified and localized early Th2 differentiation (Fig. S5 F).

Discussion

In vivo mechanisms driving early Th2 differentiation in LNs have remained enigmatic, in large part due to the complex role of TCR signaling in directing T cell effector fates and the lack of clear understanding of which molecules expressed by cDCs, or other innate cells, selectively induce Th2 polarization (Paul and Zhu, 2010). Our studies indicate that early differentiating Th2 cells undergo enhanced T cell signaling and activation, and that this is mediated through macro-clustering at the T-B border with migratory cDC2s displaying high levels of costimulatory molecules and integrin ligands but relatively low levels of surface pMHC-II. This appears to promote efficient cytokine exchange, in particular for IL-2 and IL-4, among neighboring activated T cells to reinforce localized Th2 differentiation and to support prolonged proliferation. Thus, the formation of discrete spatial microenvironments within LNs in which T cells integrate quantitatively strong activation signals from cDC2s coupled with qualitative cytokine sensing from nearby T cells promotes the initiation of large-scale Th2 responses in vivo.

Extensive evidence now exists that migratory cDC2s are required for Th2 differentiation (Gao et al., 2013; Kumamoto et al., 2013; Ochiai et al., 2014; Plantinga et al., 2013; Tussiwand et al., 2015; Williams et al., 2013). We similarly find that ablation of cDC2 maturation and migration from the skin abrogates Th2, as well as Tfh, differentiation in LNs, albeit not necessarily at the cost of reduced early T cell priming. This may be explained by the fact that in settings of ample antigen drainage with papain administration, LN resident cDCs that move into the outer paracortex are sufficient to initiate early T cell proliferation, while migratory cDC2s migrating to the T-B border induce downstream Th2 differentiation and sustain maximal expansion of responding T cells (Allenspach et al., 2008; Gatto et al., 2013; Gerner et al., 2015; Leal et al., 2021; Yi and Cyster, 2013). Notably, a recent study described a requirement for MHC-II turnover in LN resident cDCs for inducing early Th2 responses in lung draining LNs after house dust mite exposure (Castellanos

et al., 2021), suggesting that differences in DC responses between mucosal versus cutaneous barrier tissues are likely and require further study. Positioning of macro-clusters in the outer LN paracortex and near the T-B border is consistent with the localization of migratory cDC2 which move to these regions in a G-protein coupled receptor 138 (Ebi2) dependent fashion (Gatto et al., 2013; Yi and Cyster, 2013), which is potentially further influenced by CXCR5 (Krishnaswamy et al., 2017; León et al., 2012). Similarly, Ebi2 expression also likely drives early positioning and activation of CD4 T cells in the same regions (Baptista et al., 2019; Li et al., 2016). Consistent with this, the early 4get-GFP-expressing Th2 cells do not express CXCR5, indicating that this chemokine receptor is not required for early CD4 T cell localization near the T-B border. However, it is likely that the spatial proximity of macro-clusters near B cell follicles supports Tfh differentiation by enhancing the probability of interactions between those activated T cells that receive less IL-2 and neighboring B cells presenting cognate antigens, thereby explaining the involvement of migratory cDC2s in both Th2 and Tfh responses (Crotty, 2011; Eisenbarth, 2019; Krishnaswamy et al., 2017).

Factors expressed by cDC2s to selectively initiate Th2 skewing have remained unknown (Hilligan et al., 2020), but costimulatory molecule expression by cDCs can promote type-II cytokine production by in vitro stimulated T cells (Gause et al., 1997; King et al., 1995; Liu et al., 2004; Rulifson et al., 1997; Tao et al., 1997; van Rijn et al., 2004). In vivo, TSLP-driven OX40L costimulatory molecule expression by cDCs has been positively linked with Th2 responses (Ito et al., 2005; Stanbery et al., 2022; Zhou et al., 2005). Costimulatory molecules on their own do not constitute a Th2 polarizing stimulus and can be involved in promoting general T cell activation. However, we find that prolonged costimulation was less essential for adjuvant-induced Th1 responses, indicating differential requirements of costimulation for distinct helper cell lineages. Our data do support the notion that costimulation is essential for inducing IL-2 and IL-4 cytokine production and likely for eliciting IL-4R α upregulation by activated T cells to drive enhanced Th2 differentiation (Chu et al., 2014; Fraser et al., 1991; June et al., 1987; Liao et al., 2008; Liu et al., 2005; Noben-Trauth et al., 2000, 2002; Paul and Zhu, 2010). IL-2 also skews responding T cells away from the Tfh lineage, thus supporting additional specification of helper cell fate (Johnston et al., 2009, 2012; Pepper et al., 2011).

The initial cellular source of IL-4 in draining LNs has not been clearly defined, yet recently stimulated T cells can produce IL-4 in a TCR-dependent manner in vitro (Noben-Trauth et al., 2000, 2002). Mice deficient in IL-4R α also retain the capacity to secrete IL-4, suggesting that T cells are able to produce IL-4 without a requirement for prior IL-4 sensing (Noben-Trauth

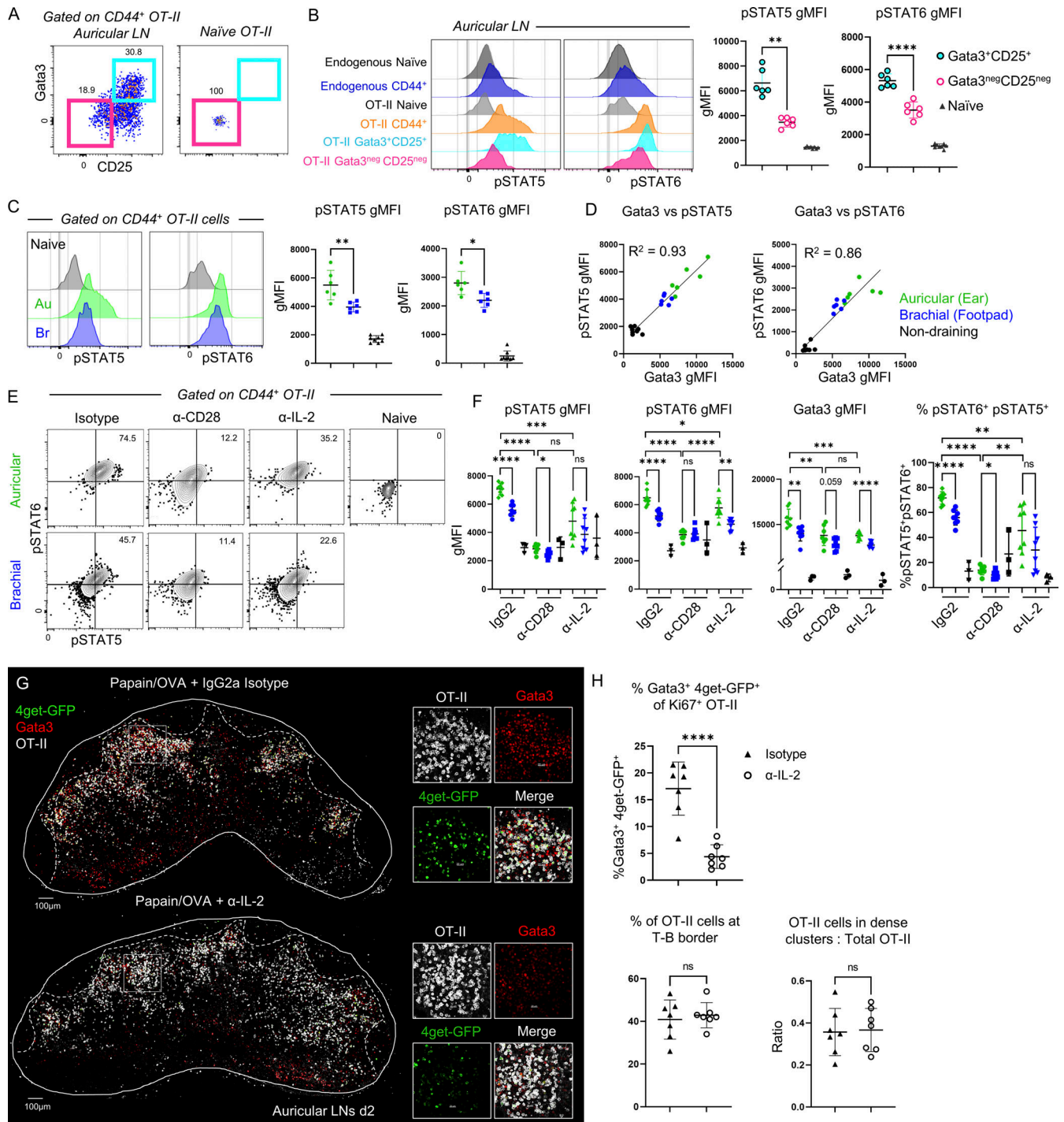


Figure 7. Increased costimulation promotes enhanced cytokine signaling and Th2 differentiation. (A–D) Naïve CD45.1 OT-II T cells were transferred to B6 mice and injected with papain OVA in the ear pinnae or front footpad. Mice were treated intraperitoneally with α -CD62L blocking antibody 6 h after immunization and dLNs were harvested and assessed by flow cytometry at 48 h. (A) Representative flow plots of Gata3 and CD25 expression on CD44⁺ or naïve OT-II cells in auricular dLNs. (B) Representative histograms and quantification of pSTAT5 and pSTAT6 staining for the indicated cell subsets within the same sample. (C) Representative histograms and quantification of pSTAT5 and pSTAT6 expression on CD44⁺ OT-II cells in auricular and brachial LNs. (D) pSTAT5 and pSTAT6 correlation with Gata3 gMFI. (E–H) Mice were treated as in A but treated intraperitoneally with α -CD28 blocking antibody, α -IL-2 blocking antibody, or IgG isotype control 24 h after immunization, and dLNs were harvested 48 h later. (E and F) Representative flow cytometry plots (E) and quantification (F) of the frequency of pSTAT5⁺ and pSTAT6⁺ cells, gMFI of pSTAT5 and pSTAT6, and Gata3 expression in CD44⁺ OT-II cells. (G) Representative images depicting OT-II macro-clustering and Th2 differentiation in auricular dLN treated with isotype control (top) or α -IL-2 blocking antibody (bottom). Gata3 signal is masked outside of Ki67⁺IRF4⁺ activated cells for visual clarity. (H) Histochemistry analysis of percent activated OT-II cells coexpressing 4get-GFP and Gata3, OT-II localization at the T–B border, and the ratio of densely clustered OT-II cells with the indicated treatment. Data shown represent one independent experiment with at least $n = 6$ independently immunized lymph nodes from three mice per group. Graphs show mean \pm SD and were analyzed using unpaired Student's t test. Paired t tests were performed when comparing responses within the same experimental tissue (panel B). **** $P < 0.0001$, *** $P < 0.001$; ** $P < 0.01$; * $P < 0.05$; $P > 0.05$ not significant (ns). Dashed lines represent T–B border. Figures are representative of two to three independent experiments.

et al., 1997). Consistent with this, IL-4 secretion by T cells can be achieved by the activation of BATF/IRF4/Jun complexes downstream of TCR engagement and costimulation in a Gata3-independent manner (Bao et al., 2016; Huber and Lohoff, 2014; Iwata et al., 2017; Krishnamoorthy et al., 2017; Kuwahara et al., 2016; Li et al., 2012; Lohoff et al., 2002; Rengarajan et al., 2002; Sahoo et al., 2015). Indeed, we observed robust expression of IRF4 and BATF in activated T cells within ear-draining auricular LNs, suggesting these transcription factors may be sufficient to induce initial IL-4 production by responding T cells within macro-clusters which can then be further amplified by canonical IL-4/IL-4R α driven Gata3 expression. While our studies do not examine other potential sources of IL-4 in LNs, the majority of activated OT-II T cells have detectable levels of pSTAT6, indicative of more widespread cytokine sensing after papain administration (Perona-Wright et al., 2010). Our findings do show that Gata3-expressing T cells located within the macro-clusters experience more extensive cytokine signaling than Gata3⁻ cells, which are outside the clusters, and this further enhances Th2 differentiation within local microenvironments. Supporting this are past observations that both IL-2 and IL-4 are secreted by T cells in a broadcasted, non-polarized fashion (Duan et al., 2021; Huse et al., 2006), as well as our results demonstrating that late CD28 blockade, which disrupts macro-clustering, results in diminished STAT phosphorylation.

Past studies have demonstrated that in vitro stimulation of CD4 T cells with strong TCR agonists or high dose of peptide promotes Th1 differentiation, while low-dose signals elicit Th2 differentiation (Bhattacharyya and Feng, 2020; Paul and Zhu, 2010; Tao et al., 1997). This has also been supported by in vivo work using peptide-pulsed DCs, which showed that TCR signal strength serves as a rheostat to control cytokine receptor expression, thus modulating the ability of T cells to sense cytokines and undergo T helper cell differentiation (van Panhuys, 2016; van Panhuys et al., 2014). Our studies are consistent with this hierarchy model, showing that cells undergoing the greatest degree of activation also receive abundant cytokines and become more differentiated. However, we show that during in vivo allergen exposure, prolonged and enhanced T activation leads to Th2 and Tfh, not Th1 polarization, and that Th1 differentiation occurs at minimal rates for these responses regardless of antigen dosage. Differences in these observations are likely explained by the fact that environmental allergens such as papain elicit inflammatory functions via proteolytic disruption of the epithelial barrier and release of the alarmin IL-33 (Cayrol et al., 2018), and this induces cDC maturation and costimulatory molecule expression through local type 2 innate lymphoid cell (ILC2) activation (Besnard et al., 2011; Halim et al., 2016; Ito et al., 2005; von Moltke and Pepper, 2018), thus necessitating in vivo administration to appropriately instruct cDCs. In addition, we and others show that during type-II inflammation, cDCs have a reduced capacity to produce the type-I skewing cytokine IL-12, thus minimizing the capacity of T cells to undergo Th1 differentiation during allergen exposure (Hilligan et al., 2020). Further, activated T cells displaying high levels of cytokine receptors appear confined within microenvironments rich in other T cells and cDC2s and away from other potential cellular

sources of IL-12, which could suppress early Th2 differentiation (Conejero et al., 2017; Everts et al., 2016). In this regard, we previously showed that papain administration does not elicit robust monocyte recruitment to the draining LNs (Leal et al., 2021), as these cells can also produce copious amounts of IL-12 during type-I inflammation (De Koker et al., 2017). Altogether, these findings suggest there is limited availability of Th1-inducing factors in draining LNs after papain administration, indicating that highly activated T cells undergoing prolonged interactions with cDCs receive Th2 polarizing cytokines in the absence of Th1-promoting factors, leading to the generation of large-scale Th2 responses. Notably, prolonged costimulatory signaling and formation of T cell macro-clusters appear far less critical for the generation of in vivo Th1 responses. This may be due to comparatively lower expression of integrin ligands by cDC2s during type-I inflammation to promote prolonged clustering, high abundance of signal 3 cytokines across vast regions of the LN parenchyma, and presence of chemokines which would drive CXCR3-expressing early Th1 cells away from sites of initial T-DC contacts (Groom et al., 2012; Leal et al., 2021).

Of note, our data also suggest that during papain exposure, antigen-bearing migratory cDC2s have low levels of pMHC complexes on the cell surface, accompanied by high amounts of costimulatory molecules and integrin ligands. Mechanisms of how type-II inflammation impacts antigen processing and presentation, as well as whether it extends to other type-II settings remains to be determined but could be driven in part by modulating the cytoskeletal properties of cDCs (Steinfelder et al., 2009). Together with TCR engagement, costimulation enhances LFA-1 integrin activation, which enables prolonged T cell-cDC interactions, as well as reduces the threshold of TCR signaling required for T cell activation, overall being consistent with our findings that low levels of pMHC-II can still lead to robust T cell responses (Wang et al., 2008). Additional integrin-mediated homotypic interactions among activated T cells may also take place, albeit likely not via ICAM-1/LFA-1 interactions. A recent study has demonstrated a role for the integrin α V β 3, for Th2 differentiation in vitro, and this integrin has also been previously linked with the migratory behavior of Th2 cells in inflamed tissues (Gaylo-Moynihan et al., 2019; Szeto et al., 2023).

A key unexpected finding in our work was that not all types of skin generated equivalent Th2 responses in the draining LNs. Our studies primarily focused on the ear versus footpad draining LNs, but additional variation across the skin is likely. A major unanswered question remains as to why cDCs within different skin sites are non-equivalently activated after exposure to the same agonist and whether this extends to other barrier tissues in mice and humans. Homeostatic tissue signals like IL-13 and IL-18 can impart cDCs and ILC2s with a tissue-specific identity, potentially reflecting intrinsic preprogramming of cDCs and other cells based on skin type residence (Halim et al., 2014; Mayer et al., 2021; Ricardo-Gonzalez et al., 2018). In addition, differences could reflect divergent DC experiences at the site of immunization. Many cytokines, including alarmins, are released from epithelial and stromal cells during type-II inflammation and barrier disruption events, yet whether these cytokines are equivalently released between skin sites requires further study.

There could be many additional tissue-specific adaptations, such as neuronal composition, mast cell differences, or divergent microbiomes which direct dermal cDC2 maturation and activation (Carroll-Portillo et al., 2015; Perner et al., 2020; Sumpter et al., 2019; Suto et al., 2006). Epidermal barrier thicknesses and other structural differences between skin sites could also contribute (Tong et al., 2015). Therefore, skin should not be thought of as a single barrier tissue but as unique compartments that may respond differently to environmental triggers. A possible evolutionary benefit of reduced Th2 responses after allergen exposure in the footpad could reflect the need for dampened inflammation in tissues with constant mechanical stress, environmental exposure, and likely damage, while still retaining the ability to induce robust Th1 responses to microbial challenges. Finally, a common feature of Th2 allergic responses is atopic march development, in which initial skin sensitization leads to downstream pathology across peripheral organs. It will thus be important to understand how different regions of the skin, the largest barrier tissue in the body, respond to allergen exposure and drive disease development.

Materials and methods

Mice

C57BL/6J, BALB/cJ, B6.Cg-Tg(Itgax-cre)1-1Reiz/J (CD11c-Cre), B6.129S1-Irf4^{tm1Rdf}/J (IRF4^{fl/fl}), and B6.129S4-Icam1^{tm1Jcgr}/J (ICAM-1.KO) were obtained from Jackson Laboratory. B6.SJL-*Ptprc^aPepc^b*/BoyCrl (CD45.1) mouse strain was obtained from Charles River Laboratory. CD45.1⁺ B6.Cg-Tg(TcraTcrb)425Cbn/J (OT-II) mice were obtained from a donating investigator (P.J. Fink, University of Washington, Seattle, WA) and crossed with CD45.2⁺ C57BL/6J mice to generate CD45.1⁺ OT-II and CD45.1⁺CD45.2⁺ OT-II lines that were used interchangeably based on recipient congenic status. The KN2 and 4get-GFP mouse strains on a B6 background were obtained from a donating investigator (M. Pepper, University of Washington). 4get-GFP and ICAM-1.KO mice were crossed to OT-II to generate 4get-GFP.OT-II and ICAM-1.KO.OT-II lines, respectively.

6–12-wk-old male and female mice were kept in specific pathogen-free (SPF) conditions at an Association for Assessment and Accreditation of Laboratory Animal Care-accredited facility at the University of Washington, South Lake Union campus. All procedures were approved by the University of Washington Institutional Animal Care and Use Committee.

Adoptive transfers

For adoptive transfers, naïve CD45.1⁺ OT-II, CD45.1⁺CD45.2⁺ OT-II, or CD45.2⁺ 4get-GFP.OT-II T cells were isolated from LNs and spleens using the naïve CD4⁺ T cell isolation kit (Miltenyi Biotec). The average purity of OT-II cells was ~75–80% for all experiments. 1×10^6 (unless otherwise noted) naïve OT-II cells were transferred into hosts intravenously via retro-orbital injection 1–3 days prior to immunization.

Immunizations and blocking antibodies

The following adjuvants and amounts per immunization site were used: 20 µg of CpG ODN 1668 (AdipoGen), Alhydrogel

(“Alum”) (Invivogen) diluted 1:1 with PBS, DBP (Sigma-Aldrich) diluted 1:1 with 100% acetone, 50 µg papain (Sigma-Aldrich), and 10 µg endotoxin-free OVA (Invivogen). In some studies, the dose of OVA given ranged from 0.1 to 100 µg per injection. For antigen presentation studies, 10 µg of LPS-free EaGFP (gift from M.K. Jenkins, University of Minnesota, Minneapolis, MN) plus 50 µg of papain were injected intradermally in the ear pinnae or the forepaw. Adjuvants were mixed with PBS in a 20 µl total volume per immunization site and injected in the hind or front footpads, subcutaneously in the flank skin, at the tail base, or intradermally in the ear pinnae (to target the popliteal, brachial, inguinal, and auricular dLNs, respectively) as indicated. For some studies, DBP was “painted” onto ear or footpad skin by pipetting 20 µl volume slowly, allowing drying between drops with the mouse under anesthesia until the liquid was completely dried. For *N.b.* infections, infectious third-stage larvae (L3) were raised and maintained as described previously (Nadsjombati et al., 2018). Mice were infected subcutaneously at the base of the tail to target the inguinal draining LN with 500 *N.b.* L3.

For in vivo antibody blocking studies, 100 µg of anti-CD62L (clone Mel-14, BioXcell) was injected intraperitoneally 6 h post immunization. In some studies, 100 µg anti-LFA-1α (clone M17/4; BioXcell), 100 µg rat IgG2a isotype control (BioXcell), 100 µg anti-CD28 (clone 37.51; BioXcell), 100 µg polyclonal Syrian hamster IgG (BioXcell), or 100 µg anti-IL-2 (clone JES6-1A12, BioXcell) was injected intraperitoneally 24 h after immunization.

Confocal microscopy

For confocal imaging, PFA-fixed and sectioned LN tissues were imaged as previously described using a Leica SP8 microscope (Germer et al., 2012). Briefly, isolated LN tissues were fixed using BD Cytofix (BD Biosciences) diluted 1:3 in PBS for 20–24 h at 4°C then dehydrated with 30% sucrose solution for 24–48 h at 4°C. LNs were then embedded in an OCT compound (Tissue-Tek) and stored at –20°C. LNs were sectioned on a Thermo Fisher Scientific Micron HM550 cryostat into 20-µm sections and stained as previously described (Germer et al., 2012). A Leica SP8 tiling confocal microscope equipped with a 40× 1.3 NA oil objective was used for image acquisition. All raw imaging data was processed and analyzed using Imaris (Bitplane).

Histocytometry and CytoMAP

Histocytometry analysis was performed as previously described (Germer et al., 2012; Leal et al., 2021). Briefly, multiparameter confocal images were corrected for fluorophore spillover using the built-in Leica Channel Dye Separation module. Single stained controls were acquired using UltraComp eBeads (Invitrogen) that were incubated with fluorescently conjugated antibodies and then mounted on slides with Fluormount-G slide mounting media (Thermo Fisher Scientific). All images were visualized and analyzed using Imaris (Bitplane). For analysis of myeloid cells, a combinatorial myeloid channel was created by adding normalized signals for CD11c, MHC-II, CD207, CD301b, and Sirpα using the Imaris XT channel arithmetic module, and this sum myeloid channel was used for myeloid isosurface object creation. For T cells, a combined activated T cell channel was created by adding normalized signals for Ki67 and IRF4. T cell

isosurface objects were next created on this channel, or in some experiments created only on Ki67 signal as indicated, and then further gated on the congenic CD45.1 or CD45.2 signal for OT-II analysis. For visual clarity in representative images, 4get-GFP signal was masked outside of CD45.2⁺ OT-II cells, and Gata3 signal was masked outside of Ki67⁺ cells. In all analyses, object statistics were exported to FlowJo software (FlowJo, LLC) for gating and phenotypic characterization. T-B border regions were manually created using B220 or MHC-II (B cell follicles) and CD3 (T cell zone) staining and represented as a surface. T-B border localization was calculated as the frequency of OT-II cells within the T-B border surface region. Clustering analysis was performed by creating isosurfaces on CD45.1 congenic signal without cell splitting. Surfaces were then filtered by volume, and surfaces exceeding 1,400 μm^3 (defining dense clusters representing ~10 or more cells) were added and presented as a ratio of dense macro-clustered surface volume (>1,400 μm^3) to total OT-II surface volume. Spatial correlation analysis was performed in CytoMAP (Stoltzfus et al., 2020). In brief, the position of all myeloid and T cell objects within LNs was used for virtual raster scanning with 50- μm radius neighborhoods. The Pearson correlation coefficient was calculated for the number of cells of different cell types within these neighborhoods. Raster-scanned neighborhoods were also used for clustering based on cell type abundance to identify distinct region types, and these regions were used for heatmap and positional visualization of regions in dLNs.

Cell isolation and flow cytometry

For myeloid cell analysis, LN tissues were mechanically disrupted and subject to digestion in PBS with 10% fetal bovine serum (FBS) with DNase I (100 $\mu\text{g}/\text{ml}$; Sigma-Aldrich), Dispase II (800 $\mu\text{g}/\text{ml}$; Sigma-Aldrich), and Collagenase P (200 $\mu\text{g}/\text{ml}$; Sigma-Aldrich) at 37°C shaking at 150 rpm for 30 min with periodic manual disruption. Flow cytometric studies of T cells in lymph nodes did not use enzymatic digestion. In some studies, mice were injected intravenously with 1 μg of anti-Thy1.2-BUV395 (clone 30-H12; BD Biosciences) ~5 min prior to sacrifice. Lung tissue was digested in complete RPMI with Liberase (70 $\mu\text{g}/\text{ml}$; Roche) and Aminoguanidine (10 mM; Sigma-Aldrich) and tissue was dissociated on the gentleMACS Dissociator (Miltenyi Biotec) as previously described (Hondowicz et al., 2016). Cell staining was conducted in the presence of Fc Block (2.4G2; Tonbo Biosciences) at 4°C for 30 min for all surface markers, except CXCR5-biotin which was stained at room temperature for 45 min. Intracellular staining was performed for 45 min at 4°C after fixation with the FXP3 Fix/perm kit (Invitrogen). In some studies, an additional permeabilization step was performed in 90% ice-cold methanol prior to intracellular staining for the detection of pSTAT5 and pSTAT6. Data were acquired on an Aurora flow cytometer (Cytek) and analyzed using FlowJo software (BD Biosciences).

CD4⁺ T cell isolation and culture

For in vitro T cell stimulation experiments, naïve CD4⁺ T cells were isolated from LNs and spleens using the naïve CD4⁺ T cell isolation kit (Miltenyi Biotec) into complete RPMI media.

400,000 cells were then plated on pretreated plates coated with the indicated concentrations of anti-CD3 ϵ (145-2C11; Thermo Fisher Scientific) and anti-CD28 (37.51; Thermo Fisher Scientific) under Th0 (anti-IFN γ 10 $\mu\text{g}/\text{ml}$; [XMG1.2, Biolegend]), or Th2 (anti-IFN γ 10 $\mu\text{g}/\text{ml}$ [XMG1.2; Biolegend] and rIL-4 50 ng/ml [Peprotech]) conditions. Cells were cultured for 48 h at 37°C and 5% CO₂ before fixation and flow cytometric analysis.

RNA sequencing

Single-cell suspensions from tissues were prepared as described above for myeloid cells. Cells were sorted from pooled dLNs from three individual mice for each group. 500 of each cDC2 cell type was sorted on an Aria III (BD Biosciences) directly into reaction buffer from the SMART-Seq v4 Ultra Low Input RNA Kit for Sequencing (Takara), and reverse transcription was performed followed by PCR amplification to generate full-length amplified cDNA. Sequencing libraries were constructed using the NexteraXT DNA sample preparation kit with unique dual indexes (Illumina) to generate Illumina-compatible barcoded libraries. Libraries were pooled and quantified using a Qubit Fluorometer (Life Technologies). Sequencing of pooled libraries was carried out on a NextSeq 2000 sequencer (Illumina) with paired-end 59-base reads using NextSeq P2 sequencing kits (Illumina) with a target depth of 5 million reads per sample. Base calls were processed to FASTQs on BaseSpace (Illumina) and a base call quality-trimming step was applied to remove low-confidence base calls from the ends of reads. The FASTQs were aligned to the GRCh38 mouse reference genome using STAR v.2.4.2a, and gene counts were generated using htseq-count. QC and metrics analysis was performed using the Picard family of tools (v1.134). Gene counts were filtered and normalized from raw counts by trimmed-mean of M values (TMM) normalization and filtered for genes expressed with at least one count per million total reads in at least 10% of the total number of libraries. Further downstream analysis was performed using publicly available RNAseq toolkits. The Degust toolkit (Powell, 2019) (v4.1.1) with integrated Voom/Limma R package was used for differentially expressed gene analysis and generation of volcano plots. Only genes with a count per million (CPM) ≥ 10 were analyzed further. Genes were filtered based on a false discovery rate cutoff ≤ 0.05 and a minimum expression fold change ≥ 2 . DEGs were input into the WebGestalt gene set analysis toolkit (Liao et al., 2019) to identify Biological Processes Gene Ontology (GO) terms and generate the associated graphs. Heatmap data tables were generated by inputting DEG data into the BIOMEX toolkit (Taverna et al., 2020). PCA plots were generated via the DEBrowser toolkit (Kucukural et al., 2019) (v1.26.3), where only genes with CPM ≥ 10 were analyzed.

Antibodies and staining reagents

Antibodies used for staining sections for confocal imaging or isolated cells for flow cytometry include the following: CD64 (clone X54-57.1; BioLegend), B220 (clone RA3-6B2; BioLegend), SIRP α (clone P84; BD Biosciences), CD11c (clone N418; BD Biosciences), CD11b (clone M1/70; BioLegend), MHCII (clone M5/114.15.2; BioLegend), IRF4 (clone IRF4.3E4; BioLegend), CD45.1 (clone A20; BioLegend), Ki67 (clone B56; BD Biosciences), Y-Ae

(clone eBioY-Ae; Thermo Fisher Scientific), Thy1.2 (clone 30-H12; BD Biosciences), CD3 (clone 17A2; BD Biosciences), Tbet (clone 4B10; BioLegend), NK1.1 (clone PK136; BioLegend), CD19 (clone 6D5; BioLegend), CD44 (clone IM7; BioLegend), XCR1 (clone ZET; BioLegend), Gata3 (clone L50-823; BD Biosciences), CXCR3 (clone CXCR3-173; BioLegend), CXCR5 (clone 2G8; BD Biosciences), pS6 (clone 2F9; Cell Signaling Technologies), PD-1 (clone RMP1-30; BioLegend), CD45.2 (clone 104; BioLegend), CD25 (clone PC61; Thermo Fisher Scientific), EpCAM (clone G8.8; Thermo Fisher Scientific), CD103 (clone M290; BD Biosciences), CD301b (clone URA-1; BioLegend), CD80 (clone 16-10A1; Thermo Fisher Scientific), CD86 (clone GL1; BD Biosciences), PDL-1 (clone MIH5; Thermo Fisher Scientific), PDL-2 (clone MIH37; BD Biosciences), BCL6 (clone KI12-91; BD Biosciences), BATF (clone D7C5 rabbit; Cell Signaling Technologies), anti-GFP (polyclonal goat; Novus Biologics), ICAM-1 (clone 3E2; BD Biosciences), CD207 (clone 929F3.01; Dendritics), CD4 (clone GK1.5; BD Biosciences), huCD2 (clone RPA-2.10; ThermoFisher Scientific), pSTAT5 (clone 47/STAT5[pY694]; BD Biosciences), pSTAT6 (clone J71-773.58.11; BD Biosciences), LIVE/DEAD Near-IR (Thermo Fisher Scientific), chicken anti-goat (Thermo Fisher Scientific), and donkey anti-rabbit (Thermo Fisher Scientific).

Statistics

Statistical analysis was performed using GraphPad Prism software. The statistical significance of differences in mean values between the two groups was analyzed by a two-tailed unpaired Student's *t* test with Welch's correction. Paired *t* tests were performed when comparing responses within the same experimental tissue. In bar graphs for all figures, data are shown as mean \pm SD. *****P* < 0.0001; ****P* < 0.001; ***P* < 0.01; **P* < 0.05; *P* > 0.05; not significant (ns). Unless otherwise noted, all data points represent independent LNs.

Online supplemental material

Fig. S1 shows the cellular composition of endogenous Th2 microenvironments after papain immunization or *N.b.* infection. Fig. S2 shows that site-specific Th2 responses are maintained across mouse strains and adjuvants. Fig. S3 shows transcriptional signatures of naïve and activated cDC2s. Fig. S4 shows the role of CD28 in T helper cell responses. Fig. S5 shows the role of LFA-1 in T helper cell response, as well as a working model.

Data availability

The data in the figures are available in the published article and the online supplemental materials. The RNA sequencing data underlying Figs. 3 and S3 are openly available at the Gene Expression Omnibus under accession no. GSE254473.

Acknowledgments

We thank current and former lab members A. de la Cruz, E. Cheng, J. Huang, J. Leal, and J. Chao for their help with conceptualizing and conducting experiments. We also thank J. von Moltke, T. Billipp, and J. McGinty for help with *Nippostrongylus brasiliensis* infections. Additionally, we thank M. Pepper, J. von Moltke, E. Tait Wojno (University of Washington), and S. Ziegler

(Benaroya Research Institute, Seattle, WA) for additional mice, reagents, and resources. Figures were created using <https://BioRender.com>.

This study was supported by National Institutes of Health (NIH) grants R01AI134713 (to M.Y. Gerner) and T32AI06677 (to M.R. Lyons-Cohen and E.A. Shamskhov), and by the National Science Foundation Graduate Research Fellowship Program under grant no. NSF DGE-1762114 (to M.R. Lyons-Cohen).

Author contributions: M.R. Lyons-Cohen and M.Y. Gerner conceptualized the study. M.R. Lyons-Cohen performed all experiments and analyzed data. E.A. Shamskhov analyzed RNA sequencing data. M.R. Lyons-Cohen and M.Y. Gerner wrote, edited, and reviewed the manuscript. M.Y. Gerner supervised the project.

Disclosures: The authors declare no competing interests exist.

Submitted: 21 July 2023

Revised: 13 December 2023

Accepted: 8 February 2024

References

- Acuto, O., and F. Michel. 2003. CD28-mediated co-stimulation: A quantitative support for TCR signalling. *Nat. Rev. Immunol.* 3:939–951. <https://doi.org/10.1038/nri1248>
- Allenspach, E.J., M.P. Lemos, P.M. Porrett, L.A. Turka, and T.M. Laufer. 2008. Migratory and lymphoid-resident dendritic cells cooperate to efficiently prime naïve CD4 T cells. *Immunity.* 29:795–806. <https://doi.org/10.1016/j.immuni.2008.08.013>
- Ataide, M.A., K. Knöpper, P. Cruz de Casas, M. Ugur, S. Eickhoff, M. Zou, H. Shaikh, A. Trivedi, A. Grafen, T. Yang, et al. 2022. Lymphatic migration of unconventional T cells promotes site-specific immunity in distinct lymph nodes. *Immunity.* 55:1813–1828.e1819. <https://doi.org/10.1016/j.immuni.2022.07.019>
- Bao, K., T. Carr, J. Wu, W. Barclay, J. Jin, M. Ciofani, and R.L. Reinhardt. 2016. BATF modulates the Th2 locus control region and regulates CD4⁺ T cell fate during antihelminth immunity. *J. Immunol.* 197:4371–4381. <https://doi.org/10.4049/jimmunol.1601371>
- Baptista, A.P., A. Gola, Y. Huang, P. Milanez-Almeida, P. Torabi-Parizi, J.F. Urban Jr., V.S. Shapiro, M.Y. Gerner, and R.N. Germain. 2019. The chemoattractant receptor Ebi2 drives intranodal naïve CD4⁺ T cell peripheralization to promote effective adaptive immunity. *Immunity.* 50:1188–1201.e6. <https://doi.org/10.1016/j.immuni.2019.04.001>
- Besnard, A.G., D. Togbe, N. Guillou, F. Erard, V. Quesniaux, and B. Ryffel. 2011. IL-33-activated dendritic cells are critical for allergic airway inflammation. *Eur. J. Immunol.* 41:1675–1686. <https://doi.org/10.1002/eji.201041033>
- Bhattacharyya, N.D., and C.G. Feng. 2020. Regulation of T Helper cell fate by TCR signal strength. *Front. Immunol.* 11:624. <https://doi.org/10.3389/fimmu.2020.00624>
- Carroll-Portillo, A., J.L. Cannon, J. te Riet, A. Holmes, Y. Kawakami, T. Kawakami, A. Cambi, and D.S. Lidke. 2015. Mast cells and dendritic cells form synapses that facilitate antigen transfer for T cell activation. *J. Cell Biol.* 210:851–864. <https://doi.org/10.1083/jcb.201412074>
- Castellanos, C.A., X. Ren, S.L. Gonzalez, H.K. Li, A.W. Schroeder, H.E. Liang, B.J. Laidlaw, D. Hu, A.C.Y. Mak, C. Eng, et al. 2021. Lymph node-resident dendritic cells drive Th2 cell development involving MARCH1. *Sci. Immunol.* 6:eabh0707. <https://doi.org/10.1126/sciimmunol.abh0707>
- Cayrol, C., A. Duval, P. Schmitt, S. Roga, M. Camus, A. Stella, O. Burlet-Schiltz, A. Gonzalez-de-Peredo, and J.P. Girard. 2018. Environmental allergens induce allergic inflammation through proteolytic maturation of IL-33. *Nat. Immunol.* 19:375–385. <https://doi.org/10.1038/s41590-018-0067-5>
- Chandler, J., M. Prout, S. Old, C. Morgan, F. Ronchese, C. Benoist, and G. Le Gros. 2022. BCL6 deletion in CD4 T cells does not affect Th2 effector mediated immunity in the skin. *Immunol. Cell Biol.* 100:791–804. <https://doi.org/10.1111/imcb.12589>

- Chen, L., and D.B. Flies. 2013. Molecular mechanisms of T cell co-stimulation and co-inhibition. *Nat. Rev. Immunol.* 13:227–242. <https://doi.org/10.1038/nri3405>
- Chu, D.K., Z. Mohammed-Ali, R. Jiménez-Saiz, T.D. Walker, S. Goncharova, A. Llop-Guevara, J. Kong, M.E. Gordon, N.G. Barra, A.E. Gillgrass, et al. 2014. T helper cell IL-4 drives intestinal Th2 priming to oral peanut antigen, under the control of OX40L and independent of innate-like lymphocytes. *Mucosal Immunol.* 7:1395–1404. <https://doi.org/10.1038/mi.2014.29>
- Conejero, L., S.C. Khoulil, S. Martínez-Cano, H.M. Izquierdo, P. Brandi, and D. Sancho. 2017. Lung CD103⁺ dendritic cells restrain allergic airway inflammation through IL-12 production. *JCI Insight.* 2:e90420. <https://doi.org/10.1172/jci.insight.90420>
- Connor, L.M., S.C. Tang, E. Cognard, S. Ochiai, K.L. Hilligan, S.I. Old, C. Pellefigues, R.F. White, D. Patel, A.A. Smith, et al. 2017. Th2 responses are primed by skin dendritic cells with distinct transcriptional profiles. *J. Exp. Med.* 214:125–142. <https://doi.org/10.1084/jem.20160470>
- Crotty, S. 2011. Follicular helper CD4 T cells (TFH). *Annu. Rev. Immunol.* 29: 621–663. <https://doi.org/10.1146/annurev-immunol-031210-101400>
- Crotty, S. 2014. T follicular helper cell differentiation, function, and roles in disease. *Immunity.* 41:529–542. <https://doi.org/10.1016/j.immuni.2014.10.004>
- De Koker, S., L. Van Hoecke, A. De Beuckelaer, K. Roose, K. Deswarte, M.A. Willart, P. Bogaert, T. Naessens, B.G. De Geest, X. Saelens, et al. 2017. Inflammatory monocytes regulate Th1 oriented immunity to CpG adjuvanted protein vaccines through production of IL-12. *Sci. Rep.* 7:5986. <https://doi.org/10.1038/s41598-017-06236-6>
- DiToro, D., C.J. Winstead, D. Pham, S. Witte, R. Andargachew, J.R. Singer, C.G. Wilson, C.L. Zindl, R.J. Luther, D.J. Silberger, et al. 2018. Differential IL-2 expression defines developmental fates of follicular versus non-follicular helper T cells. *Science.* 361:eaa02933. <https://doi.org/10.1126/science.aao2933>
- Duan, L., D. Liu, H. Chen, M.A. Mintz, M.Y. Chou, D.I. Kotov, Y. Xu, J. An, B.J. Laidlaw, and J.G. Cyster. 2021. Follicular dendritic cells restrict interleukin-4 availability in germinal centers and foster memory B cell generation. *Immunity.* 54:2256–2272.e6. <https://doi.org/10.1016/j.immuni.2021.08.028>
- Eisenbarth, S.C. 2019. Dendritic cell subsets in T cell programming: Location dictates function. *Nat. Rev. Immunol.* 19:89–103. <https://doi.org/10.1038/s41577-018-0088-1>
- Everts, B., R. Tussiwand, L. Dreesen, K.C. Fairfax, S.C. Huang, A.M. Smith, C.M. O'Neill, W.Y. Lam, B.T. Edelson, J.F. Urban Jr., et al. 2016. Migratory CD103⁺ dendritic cells suppress helminth-driven type 2 immunity through constitutive expression of IL-12. *J. Exp. Med.* 213:35–51. <https://doi.org/10.1084/jem.20150235>
- Fang, D., and J. Zhu. 2017. Dynamic balance between master transcription factors determines the fates and functions of CD4 T cell and innate lymphoid cell subsets. *J. Exp. Med.* 214:1861–1876. <https://doi.org/10.1084/jem.20170494>
- Fraser, J.D., B.A. Irving, G.R. Crabtree, and A. Weiss. 1991. Regulation of interleukin-2 gene enhancer activity by the T cell accessory molecule CD28. *Science.* 251:313–316. <https://doi.org/10.1126/science.1846244>
- Gao, Y., S.A. Nish, R. Jiang, L. Hou, P. Licona-Limón, J.S. Weinstein, H. Zhao, and R. Medzhitov. 2013. Control of T helper 2 responses by transcription factor IRF4-dependent dendritic cells. *Immunity.* 39:722–732. <https://doi.org/10.1016/j.immuni.2013.08.028>
- Gatto, D., K. Wood, I. Caminschi, D. Murphy-Durland, P. Schofield, D. Christ, G. Karupiah, and R. Brink. 2013. The chemotactic receptor EB12 regulates the homeostasis, localization and immunological function of splenic dendritic cells. *Nat. Immunol.* 14:446–453. <https://doi.org/10.1038/ni.2555>
- Gause, W.C., S.J. Chen, R.J. Greenwald, M.J. Halvorson, P. Lu, X.D. Zhou, S.C. Morris, K.P. Lee, C.H. June, F.D. Finkelman, et al. 1997. CD28 dependence of T cell differentiation to IL-4 production varies with the particular type 2 immune response. *J. Immunol.* 158:4082–4087. <https://doi.org/10.4049/jimmunol.158.9.4082>
- Gaylo-Moynihan, A., H. Prizant, M. Popović, N.R.J. Fernandes, C.S. Anderson, K.K. Chiou, H. Bell, D.C. Schrock, J. Schumacher, T. Capece, et al. 2019. Programming of distinct chemokine-dependent and -independent search strategies for Th1 and Th2 cells optimizes function at inflamed sites. *Immunity.* 51:298–309.e6. <https://doi.org/10.1016/j.immuni.2019.06.026>
- Gerner, M.Y., W. Kastenmuller, I. Ifrim, J. Kabat, and R.N. Germain. 2012. Histo-cytometry: A method for highly multiplex quantitative tissue imaging analysis applied to dendritic cell subset microanatomy in lymph nodes. *Immunity.* 37:364–376. <https://doi.org/10.1016/j.immuni.2012.07.011>
- Gerner, M.Y., P. Torabi-Parizi, and R.N. Germain. 2015. Strategically localized dendritic cells promote rapid T cell responses to lymph-borne particulate antigens. *Immunity.* 42:172–185. <https://doi.org/10.1016/j.immuni.2014.12.024>
- Groom, J.R., J. Richmond, T.T. Murooka, E.W. Sorensen, J.H. Sung, K. Bankert, U.H. von Andrian, J.J. Moon, T.R. Mempel, and A.D. Luster. 2012. CXCR3 chemokine receptor-ligand interactions in the lymph node optimize CD4⁺ T helper 1 cell differentiation. *Immunity.* 37:1091–1103. <https://doi.org/10.1016/j.immuni.2012.08.016>
- Gérard, A., A.P. Cope, C. Kemper, R. Alon, and R. Köchl. 2021. LFA-1 in T cell priming, differentiation, and effector functions. *Trends Immunol.* 42: 706–722. <https://doi.org/10.1016/j.it.2021.06.004>
- Gérard, A., O. Khan, P. Beemiller, E. Oswald, J. Hu, M. Matlobian, and M.F. Krummel. 2013. Secondary T cell-T cell synaptic interactions drive the differentiation of protective CD8⁺ T cells. *Nat. Immunol.* 14:356–363. <https://doi.org/10.1038/ni.2547>
- Halim, T.Y., Y.Y. Hwang, S.T. Scanlon, H. Zaghoulani, N. Garbi, P.G. Fallon, and A.N. McKenzie. 2016. Group 2 innate lymphoid cells license dendritic cells to potentiate memory TH2 cell responses. *Nat. Immunol.* 17: 57–64. <https://doi.org/10.1038/ni.3294>
- Halim, T.Y., C.A. Steer, L. Mathä, M.J. Gold, I. Martinez-Gonzalez, K.M. McNagny, A.N. McKenzie, and F. Takei. 2014. Group 2 innate lymphoid cells are critical for the initiation of adaptive T helper 2 cell-mediated allergic lung inflammation. *Immunity.* 40:425–435. <https://doi.org/10.1016/j.immuni.2014.01.011>
- Hilligan, K.L., S.C. Tang, E.J. Hyde, E. Roussel, J.U. Mayer, J. Yang, K.A. Wakelin, A.J. Schmidt, L.M. Connor, A. Sher, et al. 2020. Dermal IRF4⁺ dendritic cells and monocytes license CD4⁺ T helper cells to distinct cytokine profiles. *Nat. Commun.* 11:5637. <https://doi.org/10.1038/s41467-020-19463-9>
- Hondowicz, B.D., D. An, J.M. Schenkel, K.S. Kim, H.R. Steach, A.T. Krishnamurthy, G.J. Keitany, E.N. Garza, K.A. Fraser, J.J. Moon, et al. 2016. Interleukin-2-Dependent allergen-specific tissue-resident memory cells drive asthma. *Immunity.* 44:155–166. <https://doi.org/10.1016/j.immuni.2015.11.004>
- Hsieh, C.S., S.E. Macatonia, A. O'Garra, and K.M. Murphy. 1995. T cell genetic background determines default T helper phenotype development in vitro. *J. Exp. Med.* 181:713–721. <https://doi.org/10.1084/jem.181.2.713>
- Huber, M., and M. Lohoff. 2014. IRF4 at the crossroads of effector T-cell fate decision. *Eur. J. Immunol.* 44:1886–1895. <https://doi.org/10.1002/eji.201344279>
- Hung, L.Y., Y. Tanaka, K. Herbine, C. Pastore, B. Singh, A. Ferguson, N. Vora, B. Douglas, K. Zullo, E.M. Behrens, et al. 2020. Cellular context of IL-33 expression dictates impact on anti-helminth immunity. *Sci Immunol.* 5: eabc6259. <https://doi.org/10.1126/sciimmunol.abc6259>
- Huse, M., B.F. Lillemeier, M.S. Kuhns, D.S. Chen, and M.M. Davis. 2006. T cells use two directionally distinct pathways for cytokine secretion. *Nat. Immunol.* 7:247–255. <https://doi.org/10.1038/ni1304>
- Itano, A.A., S.J. McSorley, R.L. Reinhardt, B.D. Ehst, E. Ingulli, A.Y. Rudensky, and M.K. Jenkins. 2003. Distinct dendritic cell populations sequentially present antigen to CD4 T cells and stimulate different aspects of cell-mediated immunity. *Immunity.* 19:47–57. [https://doi.org/10.1016/S1074-7613\(03\)00175-4](https://doi.org/10.1016/S1074-7613(03)00175-4)
- Ito, T., Y.H. Wang, O. Duramad, T. Hori, G.J. Delespesse, N. Watanabe, F.X. Qin, Z. Yao, W. Cao, and Y.J. Liu. 2005. TSLP-activated dendritic cells induce an inflammatory T helper type 2 cell response through OX40 ligand. *J. Exp. Med.* 202:1213–1223. <https://doi.org/10.1084/jem.20051135>
- Iwata, A., V. Durai, R. Tussiwand, C.G. Briseño, X. Wu, G.E. Grajales-Reyes, T. Egawa, T.L. Murphy, and K.M. Murphy. 2017. Quality of TCR signaling determined by differential affinities of enhancers for the composite BATF-IRF4 transcription factor complex. *Nat. Immunol.* 18:563–572. <https://doi.org/10.1038/ni.3714>
- Jiang, W., M.M. Lederman, C.V. Harding, B. Rodriguez, R.J. Mohnher, and S.F. Sieg. 2007. TLR9 stimulation drives naive B cells to proliferate and to attain enhanced antigen presenting function. *Eur. J. Immunol.* 37: 2205–2213. <https://doi.org/10.1002/eji.200636984>
- Johnston, R.J., Y.S. Choi, J.A. Diamond, J.A. Yang, and S. Crotty. 2012. STAT5 is a potent negative regulator of TFH cell differentiation. *J. Exp. Med.* 209: 243–250. <https://doi.org/10.1084/jem.20111174>
- Johnston, R.J., A.C. Poholek, D. DiToro, I. Yusuf, D. Eto, B. Barnett, A.L. Dent, J. Craft, and S. Crotty. 2009. Bcl6 and Blimp-1 are reciprocal and antagonistic regulators of T follicular helper cell differentiation. *Science.* 325: 1006–1010. <https://doi.org/10.1126/science.1175870>

- June, C.H., J.A. Ledbetter, M.M. Gillespie, T. Lindsten, and C.B. Thompson. 1987. T-cell proliferation involving the CD28 pathway is associated with cyclosporine-resistant interleukin 2 gene expression. *Mol. Cell. Biol.* 7: 4472-4481. <https://doi.org/10.1128/mcb.7.12.4472-4481>
- King, C.L., R.J. Stupi, N. Craighead, C.H. June, and G. Thyphronitis. 1995. CD28 activation promotes Th2 subset differentiation by human CD4⁺ cells. *Eur. J. Immunol.* 25:587-595. <https://doi.org/10.1002/eji.1830250242>
- King, I.L., and M. Mohrs. 2009. IL-4-producing CD4⁺ T cells in reactive lymph nodes during helminth infection are T follicular helper cells. *J. Exp. Med.* 206:1001-1007. <https://doi.org/10.1084/jem.20090313>
- Krishnamoorthy, V., S. Kannanganat, M. Maienschein-Cline, S.L. Cook, J. Chen, N. Bahroos, E. Sievert, E. Corse, A. Chong, and R. Sciammas. 2017. The IRF4 gene regulatory module functions as a read-write integrator to dynamically coordinate T helper cell fate. *Immunity.* 47:481-497.e7. <https://doi.org/10.1016/j.immuni.2017.09.001>
- Krishnaswamy, J.K., U. Gowthaman, B. Zhang, J. Mattsson, L. Szeponik, D. Liu, R. Wu, T. White, S. Calabro, L. Xu, et al. 2017. Migratory CD11b⁺ conventional dendritic cells induce T follicular helper cell-dependent antibody responses. *Sci Immunol.* 2:eaam9169. <https://doi.org/10.1126/sciimmunol.aam9169>
- Krummel, M.F., J.N. Mahale, L.F.K. Uhl, E.A. Hardison, A.M. Mujal, J.M. Mazet, R.J. Weber, Z.J. Gartner, and A. Gérard. 2018. Paracrine costimulation of IFN- γ signaling by integrins modulates CD8 T cell differentiation. *Proc. Natl. Acad. Sci. USA.* 115:11585-11590. <https://doi.org/10.1073/pnas.1804556115>
- Kucukural, A., O. Yukselen, D.M. Ozata, M.J. Moore, and M. Garber. 2019. DEBrowser: Interactive differential expression analysis and visualization tool for count data. *BMC Genomics.* 20:6. <https://doi.org/10.1186/s12864-018-5362-x>
- Kumamoto, Y., M. Linehan, J.S. Weinstein, B.J. Laidlaw, J.E. Craft, and A. Iwasaki. 2013. CD301b⁺ dermal dendritic cells drive T helper 2 cell-mediated immunity. *Immunity.* 39:733-743. <https://doi.org/10.1016/j.immuni.2013.08.029>
- Kuwahara, M., W. Ise, M. Ochi, J. Suzuki, K. Kometani, S. Maruyama, M. Izumoto, A. Matsumoto, N. Takemori, A. Takemori, et al. 2016. Bach2-Batf interactions control Th2-type immune response by regulating the IL-4 amplification loop. *Nat. Commun.* 7:12596. <https://doi.org/10.1038/ncomms12596>
- Larson, R.P., S.C. Zimmerli, M.R. Comeau, A. Itano, M. Omori, M. Iseki, C. Hauser, and S.F. Ziegler. 2010. Dibutyl phthalate-induced thymic stromal lymphopoietin is required for Th2 contact hypersensitivity responses. *J. Immunol.* 184:2974-2984. <https://doi.org/10.4049/jimmunol.0803478>
- Leal, J.M., J.Y. Huang, K. Kohli, C. Stoltzfus, M.R. Lyons-Cohen, B.E. Olin, M. Gale, and M.Y. Gerner. 2021. Innate cell microenvironments in lymph nodes shape the generation of T cell responses during type I inflammation. *Sci Immunol.* 6:eabb9435. <https://doi.org/10.1126/sciimmunol.abb9435>
- León, B. 2023. A model of Th2 differentiation based on polarizing cytokine repression. *Trends Immunol.* 44:399-407. <https://doi.org/10.1016/j.it.2023.04.004>
- León, B., A. Ballesteros-Tato, J.L. Browning, R. Dunn, T.D. Randall, and F.E. Lund. 2012. Regulation of T(H)2 development by CXCR5⁺ dendritic cells and lymphotoxin-expressing B cells. *Nat. Immunol.* 13:681-690. <https://doi.org/10.1038/ni.2309>
- Li, J., E. Lu, T. Yi, and J.G. Cyster. 2016. EB12 augments Tfh cell fate by promoting interaction with IL-2- quenching dendritic cells. *Nature.* 533:110-114. <https://doi.org/10.1038/nature17947>
- Li, P., R. Spolski, W. Liao, L. Wang, T.L. Murphy, K.M. Murphy, and W.J. Leonard. 2012. BATF-JUN is critical for IRF4-mediated transcription in T cells. *Nature.* 490:543-546. <https://doi.org/10.1038/nature11530>
- Liao, W., D.E. Schones, J. Oh, Y. Cui, K. Cui, T.Y. Roh, K. Zhao, and W.J. Leonard. 2008. Priming for T helper type 2 differentiation by interleukin 2-mediated induction of interleukin 4 receptor alpha-chain expression. *Nat. Immunol.* 9:1288-1296. <https://doi.org/10.1038/ni.1656>
- Liao, Y., J. Wang, E.J. Jaehnig, Z. Shi, and B. Zhang. 2019. WebGestalt 2019: Gene set analysis toolkit with revamped UIs and APIs. *Nucleic Acids Res.* 47:W199-W205. <https://doi.org/10.1093/nar/gkz401>
- Liu, Z., Q. Liu, H. Hamed, R.M. Anthony, A. Foster, F.D. Finkelman, J.F. Urban Jr., and W.C. Gause. 2005. IL-2 and autocrine IL-4 drive the in vivo development of antigen-specific Th2 T cells elicited by nematode parasites. *J. Immunol.* 174:2242-2249. <https://doi.org/10.4049/jimmunol.174.4.2242>
- Liu, Z., Q. Liu, J. Pesce, R.M. Anthony, E. Lamb, J. Whitmire, H. Hamed, M. Morimoto, J.F. Urban Jr., and W.C. Gause. 2004. Requirements for the development of IL-4-producing T cells during intestinal nematode infections: What it takes to make a Th2 cell in vivo. *Immunol. Rev.* 201:57-74. <https://doi.org/10.1111/j.0105-2896.2004.00186.x>
- Lohoff, M., H.W. Mittrücker, S. Prechtel, S. Bischof, F. Sommer, S. Kock, D.A. Ferrick, G.S. Duncan, A. Gessner, and T.W. Mak. 2002. Dysregulated T helper cell differentiation in the absence of interferon regulatory factor 4. *Proc. Natl. Acad. Sci. USA.* 99:11808-11812. <https://doi.org/10.1073/pnas.182425099>
- Mayer, J.U., K.L. Hilligan, J.S. Chandler, D.A. Eccles, S.I. Old, R.G. Domingues, J. Yang, G.R. Webb, L. Munoz-Erazo, E.J. Hyde, et al. 2021. Homeostatic IL-13 in healthy skin directs dendritic cell differentiation to promote T_H2 and inhibit T_H17 cell polarization. *Nat. Immunol.* 22:1538-1550. <https://doi.org/10.1038/s41590-021-01067-0>
- Mempel, T.R., S.E. Henrickson, and U.H. Von Andrian. 2004. T-cell priming by dendritic cells in lymph nodes occurs in three distinct phases. *Nature.* 427:154-159. <https://doi.org/10.1038/nature02238>
- Mohrs, K., A.E. Wakil, N. Killeen, R.M. Locksley, and M. Mohrs. 2005. A two-step process for cytokine production revealed by IL-4 dual-reporter mice. *Immunity.* 23:419-429. <https://doi.org/10.1016/j.immuni.2005.09.006>
- Mohrs, M., K. Shinkai, K. Mohrs, and R.M. Locksley. 2001. Analysis of type 2 immunity in vivo with a bicistronic IL-4 reporter. *Immunity.* 15:303-311. [https://doi.org/10.1016/S1074-7613\(01\)00186-8](https://doi.org/10.1016/S1074-7613(01)00186-8)
- Nadjsombati, M.S., J.W. McGinty, M.R. Lyons-Cohen, J.B. Jaffe, L. DiPeso, C. Schneider, C.N. Miller, J.L. Pollack, G.A. Nagana Gowda, M.F. Fontana, et al. 2018. Detection of succinate by intestinal Tuft cells triggers a type 2 innate immune circuit. *Immunity.* 49:33-41.e7. <https://doi.org/10.1016/j.immuni.2018.06.016>
- Noben-Trauth, N., J. Hu-Li, and W.E. Paul. 2000. Conventional, naive CD4⁺ T cells provide an initial source of IL-4 during Th2 differentiation. *J. Immunol.* 165:3620-3625. <https://doi.org/10.4049/jimmunol.165.7.3620>
- Noben-Trauth, N., J. Hu-Li, and W.E. Paul. 2002. IL-4 secreted from individual naive CD4⁺ T cells acts in an autocrine manner to induce Th2 differentiation. *Eur. J. Immunol.* 32:1428-1433. [https://doi.org/10.1002/1521-4141\(200205\)32:5<1428::AID-IMMU1428>3.0.CO;2-0](https://doi.org/10.1002/1521-4141(200205)32:5<1428::AID-IMMU1428>3.0.CO;2-0)
- Noben-Trauth, N., L.D. Shultz, F. Brombacher, J.F. Urban Jr., H. Gu, and W.E. Paul. 1997. An interleukin 4 (IL-4)-independent pathway for CD4⁺ T cell IL-4 production is revealed in IL-4 receptor-deficient mice. *Proc. Natl. Acad. Sci. USA.* 94:10838-10843. <https://doi.org/10.1073/pnas.94.20.10838>
- Ochiai, S., B. Roediger, A. Abtin, E. Shklovskaya, B. Fazekas de St Groth, H. Yamane, W. Weninger, G. Le Gros, and F. Ronchese. 2014. CD326(lo)CD103(lo)CD11b(lo) dermal dendritic cells are activated by thymic stromal lymphopoietin during contact sensitization in mice. *J. Immunol.* 193:2504-2511. <https://doi.org/10.4049/jimmunol.1400536>
- Paul, W.E., and J. Zhu. 2010. How are T(H)2-type immune responses initiated and amplified? *Nat. Rev. Immunol.* 10:225-235. <https://doi.org/10.1038/nri2735>
- Pepper, M., A.J. Pagán, B.Z. Igyártó, J.J. Taylor, and M.K. Jenkins. 2011. Opposing signals from the Bcl6 transcription factor and the interleukin-2 receptor generate T helper 1 central and effector memory cells. *Immunity.* 35:583-595. <https://doi.org/10.1016/j.immuni.2011.09.009>
- Perner, C., C.H. Flayer, X. Zhu, P.A. Aderhold, Z.N.A. Dewan, T. Voisin, R.B. Camire, O.A. Chow, I.M. Chiu, and C.L. Sokol. 2020. Substance P release by sensory neurons triggers dendritic cell migration and initiates the type-2 immune response to allergens. *Immunity.* 53:1063-1077.e7. <https://doi.org/10.1016/j.immuni.2020.10.001>
- Perona-Wright, G., K. Mohrs, and M. Mohrs. 2010. Sustained signaling by canonical helper T cell cytokines throughout the reactive lymph node. *Nat. Immunol.* 11:520-526. <https://doi.org/10.1038/ni.1866>
- Plantinga, M., M. Williams, M. Vanheerswynghels, K. Deswarte, F. Branco-Madeira, W. Toussaint, L. Vanhoutte, K. Neyt, N. Killeen, B. Malissen, et al. 2013. Conventional and monocyte-derived CD11b(+) dendritic cells initiate and maintain T helper 2 cell-mediated immunity to house dust mite allergen. *Immunity.* 38:322-335. <https://doi.org/10.1016/j.immuni.2012.10.016>
- Poholek, A.C. 2021. Tissue-specific contributions to control of T cell immunity. *Immunohorizons.* 5:410-423. <https://doi.org/10.4049/immunohorizons.2000103>
- Powell, D. 2019. drpowell/degust.4.1.1 (4.1.1). *Zenodo.* <https://doi.org/10.5281/zenodo.3501067>
- Prout, M.S., R.L. Kyle, F. Ronchese, and G. Le Gros. 2018. IL-4 is a key requirement for IL-4- and IL-4/IL-13-expressing CD4 Th2 subsets in lung and skin. *Front. Immunol.* 9:1211. <https://doi.org/10.3389/fimmu.2018.01211>

- Randolph, D.A., G. Huang, C.J. Carruthers, L.E. Bromley, and D.D. Chaplin. 1999. The role of CCR7 in TH1 and TH2 cell localization and delivery of B cell help in vivo. *Science*. 286:2159–2162. <https://doi.org/10.1126/science.286.5447.2159>
- Rengarajan, J., K.A. Mowen, K.D. McBride, E.D. Smith, H. Singh, and L.H. Glimcher. 2002. Interferon regulatory factor 4 (IRF4) interacts with NFATc2 to modulate interleukin 4 gene expression. *J. Exp. Med.* 195: 1003–1012. <https://doi.org/10.1084/jem.20011128>
- Ricardo-Gonzalez, R.R., S.J. Van Dyken, C. Schneider, J. Lee, J.C. Nussbaum, H.E. Liang, D. Vaka, W.L. Eckalbar, A.B. Molofsky, D.J. Erle, and R.M. Locksley. 2018. Tissue signals imprint ILC2 identity with anticipatory function. *Nat. Immunol.* 19:1093–1099. <https://doi.org/10.1038/s41590-018-0201-4>
- Rulifson, I.C., A.I. Sperling, P.E. Fields, F.W. Fitch, and J.A. Bluestone. 1997. CD28 costimulation promotes the production of Th2 cytokines. *J. Immunol.* 158:658–665. <https://doi.org/10.4049/jimmunol.158.2.658>
- Ruterbusch, M., K.B. Pruner, L. Shehata, and M. Pepper. 2020. In vivo CD4⁺ T cell differentiation and function: Revisiting the Th1/Th2 paradigm. *Annu. Rev. Immunol.* 38:705–725. <https://doi.org/10.1146/annurev-immunol-103019-085803>
- Sabatos, C.A., J. Doh, S. Chakravarti, R.S. Friedman, P.G. Pandurangi, A.J. Tooley, and M.F. Krummel. 2008. A synaptic basis for paracrine interleukin-2 signaling during homotypic T cell interaction. *Immunity*. 29:238–248. <https://doi.org/10.1016/j.immuni.2008.05.017>
- Sahoo, A., A. Alekseev, K. Tanaka, L. Obertas, B. Lerman, C. Haymaker, K. Clise-Dwyer, J.S. McMurray, and R. Nurieva. 2015. Batf is important for IL-4 expression in T follicular helper cells. *Nat. Commun.* 6:7997. <https://doi.org/10.1038/ncomms8997>
- Stanbery, A.G., Shuchi Smita, E.D. Jakob von Moltke, Tait Wojno, and S.F. Ziegler. 2022. TSLP, IL-33, and IL-25: Not just for allergy and helminth infection. *J. Allergy Clin. Immunol.* 150:1302–1313. <https://doi.org/10.1016/j.jaci.2022.07.003>
- Steinfelder, S., J.F. Andersen, J.L. Cannons, C.G. Feng, M. Joshi, D. Dwyer, P. Caspar, P.L. Schwartzberg, A. Sher, and D. Jankovic. 2009. The major component in schistosome eggs responsible for conditioning dendritic cells for Th2 polarization is a T2 ribonuclease (omega-1). *J. Exp. Med.* 206:1681–1690. <https://doi.org/10.1084/jem.20082462>
- Stoltzfus, C.R., J. Filipek, B.H. Gern, B.E. Olin, J.M. Leal, Y. Wu, M.R. Lyons-Cohen, J.Y. Huang, C.L. Paz-Stoltzfus, C.R. Plumlee, et al. 2020. CytoMAP: A spatial analysis toolbox reveals features of myeloid cell organization in lymphoid tissues. *Cell Rep.* 31:107523. <https://doi.org/10.1016/j.celrep.2020.107523>
- Sumpter, T.L., S.C. Balmert, and D.H. Kaplan. 2019. Cutaneous immune responses mediated by dendritic cells and mast cells. *JCI Insight*. 4:e123947. <https://doi.org/10.1172/jci.insight.123947>
- Suto, H., S. Nakae, M. Kakurai, J.D. Sedgwick, M. Tsai, and S.J. Galli. 2006. Mast cell-associated TNF promotes dendritic cell migration. *J. Immunol.* 176:4102–4112. <https://doi.org/10.4049/jimmunol.176.7.4102>
- Szeto, A.C.H., A.C.F. Ferreira, J. Mannion, P.A. Clark, M. Sivasubramaniam, M.W.D. Heycock, A. Crisp, H.E. Jolin, P. Kozik, M.D. Knolle, and A.N.J. McKenzie. 2023. An $\alpha v\beta 3$ integrin checkpoint is critical for efficient TH2 cell cytokine polarization and potentiation of antigen-specific immunity. *Nat. Immunol.* 24:123–135. <https://doi.org/10.1038/s41590-022-01378-w>
- Tao, X., S. Constant, P. Jorritsma, and K. Bottomly. 1997. Strength of TCR signal determines the costimulatory requirements for Th1 and Th2 CD4⁺ T cell differentiation. *J. Immunol.* 159:5956–5963. <https://doi.org/10.4049/jimmunol.159.12.5956>
- Taverna, F., J. Goveia, T.K. Karakach, S. Khan, K. Rohlenova, L. Treps, A. Subramanian, L. Schoonjans, M. Dewerchin, G. Eelen, and P. Carmeliet. 2020. BIOMEX: An interactive workflow for (single cell) omics data interpretation and visualization. *Nucleic Acids Res.* 48:W385–W394. <https://doi.org/10.1093/nar/gkaa332>
- Tong, P.L., B. Roediger, N. Kolesnikoff, M. Biro, S.S. Tay, R. Jain, L.E. Shaw, M.A. Grimbaldston, and W. Weninger. 2015. The skin immune atlas: Three-dimensional analysis of cutaneous leukocyte subsets by multiphoton microscopy. *J. Invest. Dermatol.* 135:84–93. <https://doi.org/10.1038/jid.2014.289>
- Tussiwand, R., B. Everts, G.E. Grajales-Reyes, N.M. Kretzer, A. Iwata, J. Bagaitkar, X. Wu, R. Wong, D.A. Anderson, T.L. Murphy, et al. 2015. Klf4 expression in conventional dendritic cells is required for T helper 2 cell responses. *Immunity*. 42:916–928. <https://doi.org/10.1016/j.immuni.2015.04.017>
- van Panhuys, N. 2016. TCR signal strength alters T-DC activation and interaction times and directs the outcome of differentiation. *Front. Immunol.* 7:6. <https://doi.org/10.3389/fimmu.2016.00006>
- van Panhuys, N., F. Klauschen, and R.N. Germain. 2014. T-cell-receptor-dependent signal intensity dominantly controls CD4(+) T cell polarization in vivo. *Immunity*. 41:63–74. <https://doi.org/10.1016/j.immuni.2014.06.003>
- van Rijt, L.S., N. Vos, M. Willart, A. Kleinjan, A.J. Coyle, H.C. Hoogsteden, and B.N. Lambrecht. 2004. Essential role of dendritic cell CD80/CD86 costimulation in the induction, but not reactivation, of TH2 effector responses in a mouse model of asthma. *J. Allergy Clin. Immunol.* 114: 166–173. <https://doi.org/10.1016/j.jaci.2004.03.044>
- von Moltke, J., M. Ji, H.E. Liang, and R.M. Locksley. 2016. Tuft-cell-derived IL-25 regulates an intestinal ILC2-epithelial response circuit. *Nature*. 529:221–225. <https://doi.org/10.1038/nature16161>
- von Moltke, J., and M. Pepper. 2018. Sentinels of the type 2 immune response. *Trends Immunol.* 39:99–111. <https://doi.org/10.1016/j.it.2017.10.004>
- Walker, J.A., and A.N.J. McKenzie. 2018. TH2 cell development and function. *Nat. Rev. Immunol.* 18:121–133. <https://doi.org/10.1038/nri.2017.118>
- Wang, Y., K. Shibuya, Y. Yamashita, J. Shirakawa, K. Shibata, H. Kai, T. Yokosuka, T. Saito, S. Honda, S. Tahara-Hanaoka, and A. Shibuya. 2008. LFA-1 decreases the antigen dose for T cell activation in vivo. *Int. Immunol.* 20:1119–1127. <https://doi.org/10.1093/intimm/dxn070>
- Williams, J.W., M.Y. Tjota, B.S. Clay, B. Vander Lugt, H.S. Bandukwala, C.L. Hrusch, D.C. Decker, K.M. Blaine, B.R. Fixsen, H. Singh, et al. 2013. Transcription factor IRF4 drives dendritic cells to promote Th2 differentiation. *Nat. Commun.* 4:2990. <https://doi.org/10.1038/ncomms3990>
- Yi, T., and J.G. Cyster. 2013. EB12-mediated bridging channel positioning supports splenic dendritic cell homeostasis and particulate antigen capture. *Elife*. 2:e00757. <https://doi.org/10.7554/eLife.00757>
- Yin, X., S. Chen, and S.C. Eisenbarth. 2021. Dendritic cell regulation of T helper cells. *Annu. Rev. Immunol.* 39:759–790. <https://doi.org/10.1146/annurev-immunol-101819-025146>
- Zhou, B., M.R. Comeau, T. De Smedt, H.D. Liggitt, M.E. Dahl, D.B. Lewis, D. Gyarmati, T. Aye, D.J. Campbell, and S.F. Ziegler. 2005. Thymic stromal lymphopoietin as a key initiator of allergic airway inflammation in mice. *Nat. Immunol.* 6:1047–1053. <https://doi.org/10.1038/ni1247>
- Zhu, J., D. Jankovic, A.J. Oler, G. Wei, S. Sharma, G. Hu, L. Guo, R. Yagi, H. Yamane, G. Punkosdy, et al. 2012. The transcription factor T-bet is induced by multiple pathways and prevents an endogenous Th2 cell program during Th1 cell responses. *Immunity*. 37:660–673. <https://doi.org/10.1016/j.immuni.2012.09.007>

Supplemental material

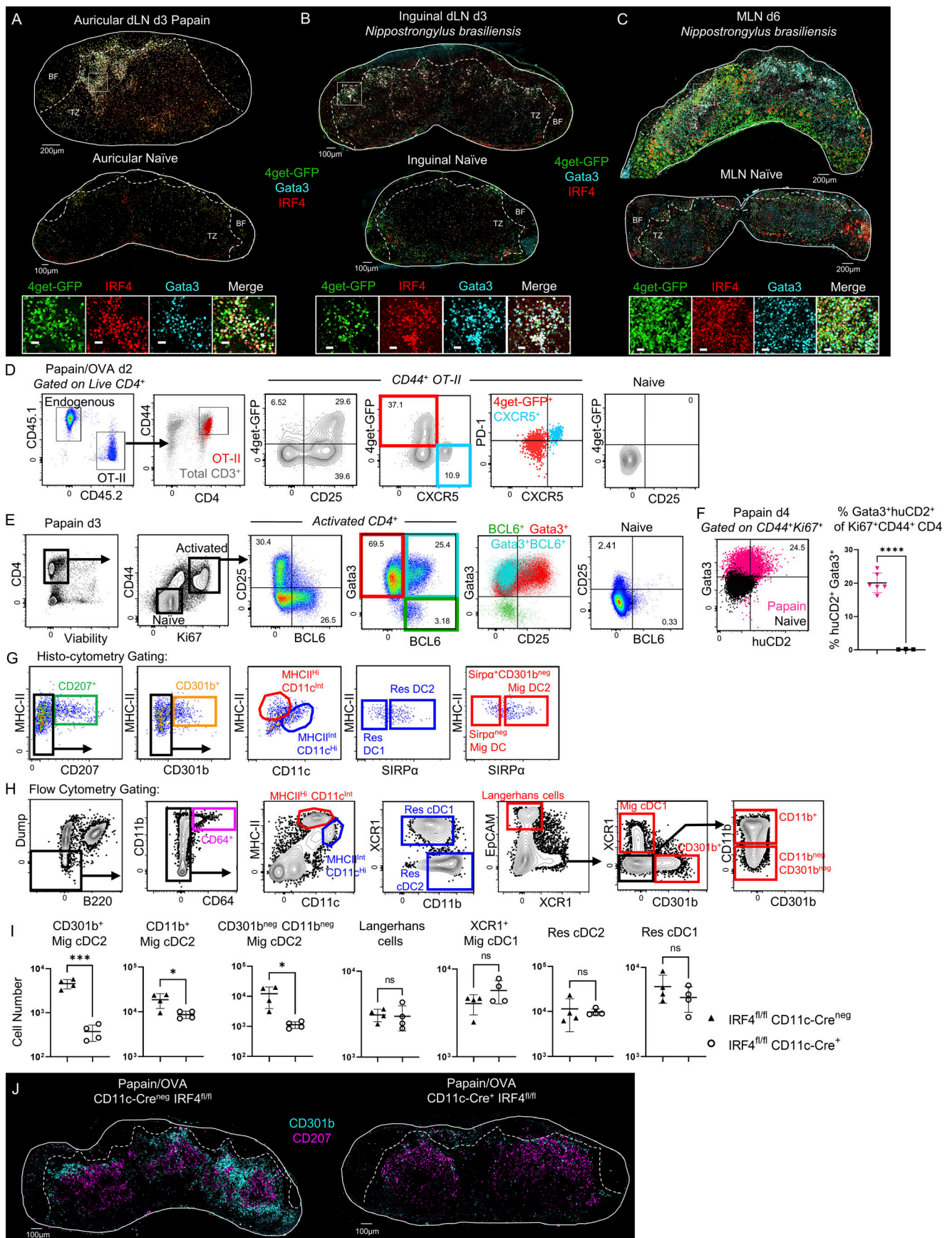


Figure S1. **Cellular composition of Th2 microenvironments after papain immunization or *N.b.* infection.** **(A)** 4get-GFP mice were immunized in the ear pinnae with papain, and auricular dLNs or naïve LNs was harvested for confocal microscopy 3 days later. Representative images and zoom-ins with the indicated markers are shown. **(B and C)** 4get-GFP mice were inoculated subcutaneously at the tail base with 500 *N.b.* L3 larvae and the draining inguinal LNs and mesenteric LN (MLN), or LNs from naïve mice, were harvested 3 or 6 days later, respectively, for confocal microscopy. Representative images and zoom-ins depicting Th2 macro-clustering with the indicated markers are shown. **(D)** Naïve CD45.2 4get.OT-II T cells were transferred to CD45.1 mice and injected with papain OVA in the ear pinnae, treated with α -CD62L blocking antibody at 6 h, and harvested for flow cytometry 48 h later. Representative gating for T follicular helper (Tfh) and T effector (Teff) OT-II cells is shown with the indicated markers. **(E)** B6 mice were immunized with papain in the ear pinnae and auricular dLNs were harvested 3 days later for flow cytometry. Representative gating for endogenous T cell activation is shown with Gata3, BCL6, and CD25 identifying Tfh and Teff T cells. **(F)** $KN2^{+/-}$ mice were immunized with papain in the ear pinnae and auricular dLNs or naïve LNs were harvested 4 days later for flow cytometry. Representative flow cytometry plot and quantification of huCD2 and Gata3 expression is shown. **(G and H)** Representative gating schemes for histocytometry (G) or flow cytometry (H) analysis of myeloid cells. **(I and J)** $CD11c-Cre^{+} Irf4^{fl/fl}$ or $CD11c-Cre^{-} Irf4^{fl/fl}$ were immunized with papain in the ear pinnae and dLNs were harvested 2 days later for flow cytometry or confocal microscopy. **(I)** Quantification of the indicated myeloid cell subsets is shown. **(J)** Representative images depicting $CD301b^{+}$ and $CD207^{+}$ cell localization in dLNs. Data shown represents one independent experiment with at least $n = 4$ independently immunized lymph nodes from two mice per group. Graphs show mean \pm SD and were analyzed using unpaired Student's *t* test. **** $P < 0.0001$; *** $P < 0.001$; ** $P < 0.01$; * $P < 0.05$; $P > 0.05$ not significant (ns). BF = B cell follicles; TZ = T cell zone. Dashed lines represent T–B border. Inset scale bars represent 20 μ m. A and D–H are representative of five independent experiments. B, C, I, and J are representative of two to three independent experiments.

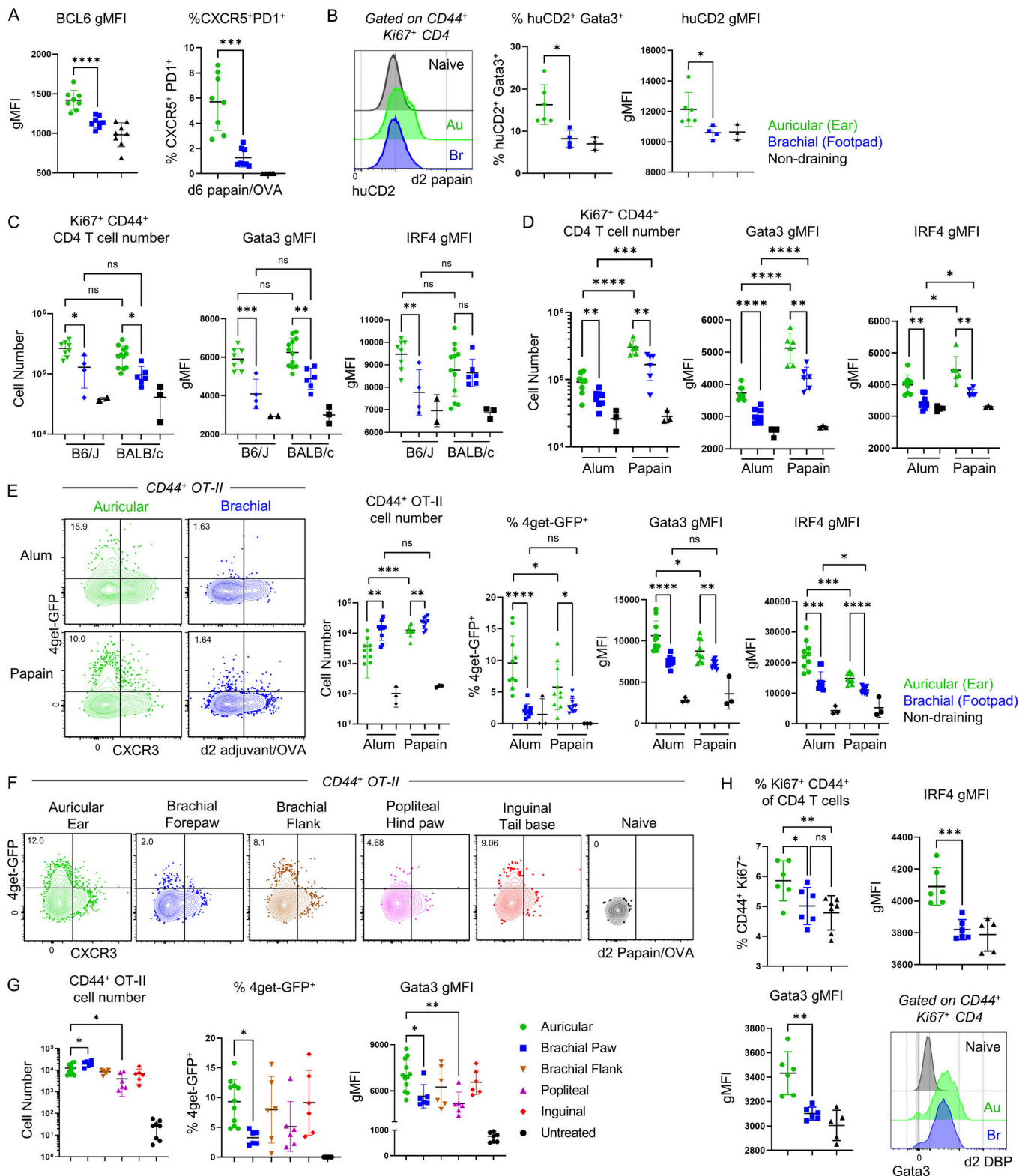


Figure S2. **Site-specific Th2 responses are maintained across mouse strains and adjuvants.** (A) 0.5×10^6 naive CD45.2 4get.OT-II cells were transferred to CD45.1 mice and injected with papain OVA in the ear pinnae or front footpad and dLNs, spleen, and lung were harvested and assessed by flow cytometry 6 days later. BCL6 gMFI and frequency of CXCR5⁺PD-1⁺ of CD44⁺ OT-II cells are shown. (B) KN2^{-/-} mice were immunized with papain in the ear pinnae or front footpad and dLNs were assessed by flow cytometry 2 days later. Representative histogram and frequency of KN2⁺Gata3⁺ and KN2 gMFI of CD44⁺Ki67⁺ CD4 cells are shown. (C) B6 or Balb/c mice were immunized in the ear pinnae and front footpad with papain and dLNs were harvested at day 3 for flow cytometry. CD44⁺Ki67⁺ T cell number, and Gata3 and IRF4 gMFI of CD44⁺Ki67⁺ T cells are shown. (D) B6 mice were immunized in the ear pinnae and front footpad with papain or Alum OVA and dLNs were harvested on day 3 for flow cytometry. CD44⁺Ki67⁺ T cell number, and Gata3 and IRF4 gMFI of CD44⁺Ki67⁺ T cells are

shown. **(E–G)** Naïve CD45.2 4get.OT-II cells were transferred to CD45.1 mice, injected with the indicated adjuvants plus OVA in the ear pinnae or front footpad, treated intraperitoneally with α -CD62L 6 h post immunization and dLNs were harvested and assessed by flow cytometry at 48 h. **(E)** Representative flow plots, CD44⁺ OT-II cell number, frequency of 4get-GFP⁺ cells, and Gata3 and IRF4 gMFI of CD44⁺ OT-II cells after immunization with the indicated adjuvants are shown. **(F and G)** Mice were treated as above but injected with papain OVA in the ear pinnae, front footpad, hind footpad, dorsal flank skin, or tail base and the corresponding dLNs were harvested for flow cytometry 2 days later. Representative flow plots, CD44⁺ OT-II cell number, and the frequency of 4get-GFP⁺ cells and Gata3 gMFI of CD44⁺ OT-II cells are shown. **(H)** DBP was topically applied (painted) onto the ear or front footpad skin of B6 mice and dLNs were harvested for flow cytometry 48 h later. The frequency of CD44⁺Ki67⁺ T cells, and Gata3 and IRF4 gMFI of CD44⁺Ki67⁺ T cells is shown. Data shown represents one independent experiment with at least $n = 4$ independently immunized lymph nodes from two mice per group. Graphs show mean \pm SD and were analyzed using unpaired Student's *t* test. **** $P < 0.0001$; *** $P < 0.001$; ** $P < 0.01$; * $P < 0.05$; $P > 0.05$ not significant (ns). A–G are representative of two to three independent experiments. H is representative of four independent experiments.

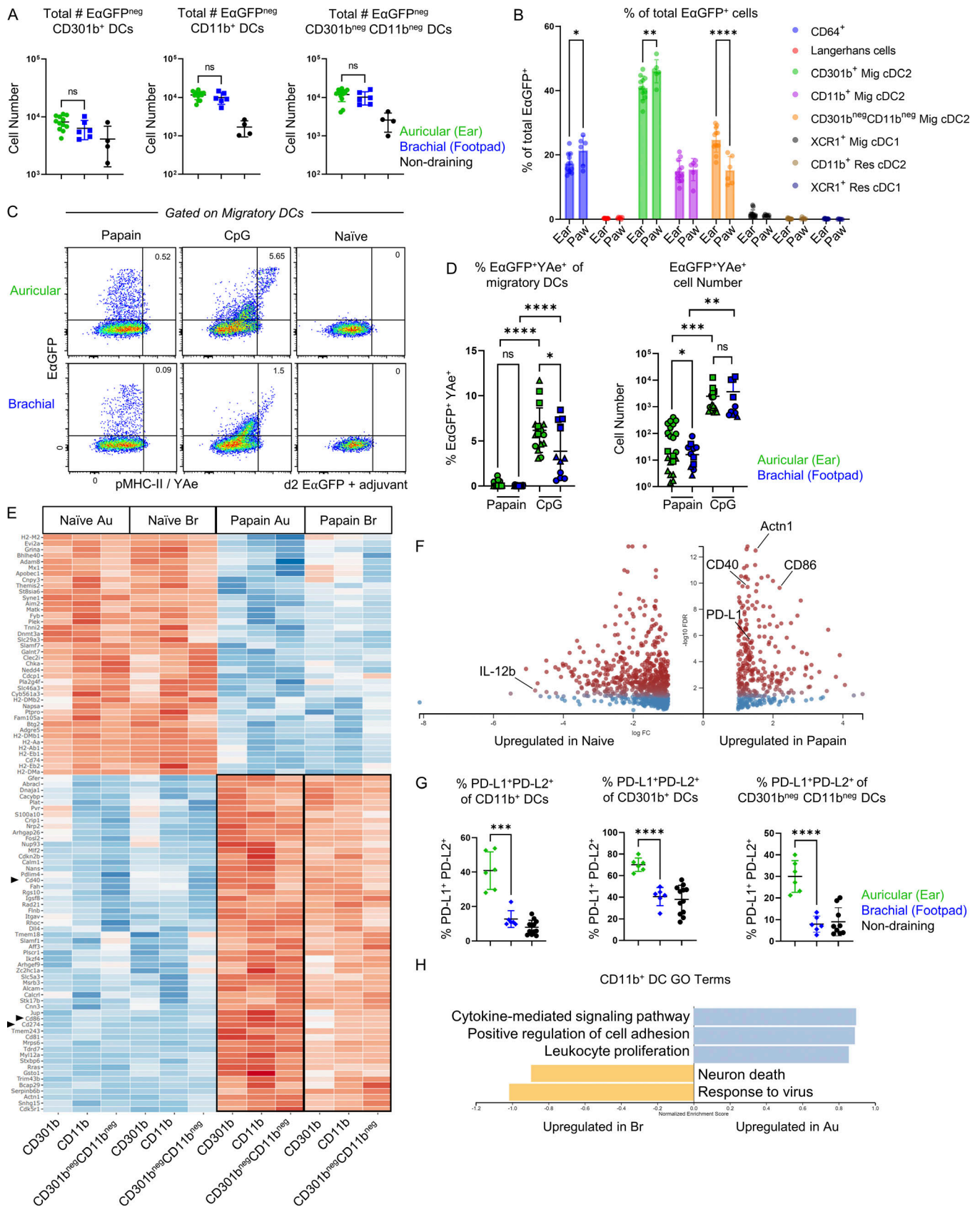


Figure S3. **Transcriptional signatures of naive and activated cDC2s.** (A–D) B6 mice were immunized in the ear pinnae or front footpad with papain or CpG plus EαGFP as indicated and harvested for flow cytometry 48 h later. (A) Total number of EαGFP⁺ cells for the indicated DC subsets. (B) Frequency of total EαGFP⁺ cells of the indicated cell subsets. (C and D) Representative flow plots (C) and quantification (D) showing EαGFP and YAe expression on migratory DCs

after immunization with the indicated adjuvant. **(E and F)** EαGFP⁺ cDC2 populations were sorted from dLNs on day 2 for bulk RNA sequencing as in Fig. 3 D. **(E)** Heatmap of all DEGs with a FDR < 0.05 and >2× fold change between naïve and papain immunized DCs from auricular and brachial LNs is shown. **(F)** Volcano plot of DEGs between papain immunized and naïve DCs from auricular and brachial dLNs. Red indicates a FDR < 0.05. Genes with a log fold change >2 are shown. **(G)** Migratory DCs were assessed for surface PD-L1 and PD-L2 expression 2 days after papain immunization by flow cytometry. Quantification of the frequency of PD-L1⁺ PD-L2⁺ for the indicated DC subsets is shown. **(H)** GO biological process term enrichment analysis based on all DEGs in EαGFP⁺ CD11b⁺ DC populations between auricular and brachial dLNs. Data shown represents one independent experiment with at least *n* = 6 independently immunized lymph nodes from three mice per group. Data from multiple pooled experiments are denoted by different symbols within the same group. Graphs show mean ± SD and were analyzed using unpaired Student's *t* test. *****P* < 0.0001; ****P* < 0.001; ***P* < 0.01; **P* < 0.05; *P* > 0.05 not significant (ns). A–D and G are representative of three independent experiments. E, F, and H are representative of one independent RNA sequencing experiment with *n* = 3 per group.

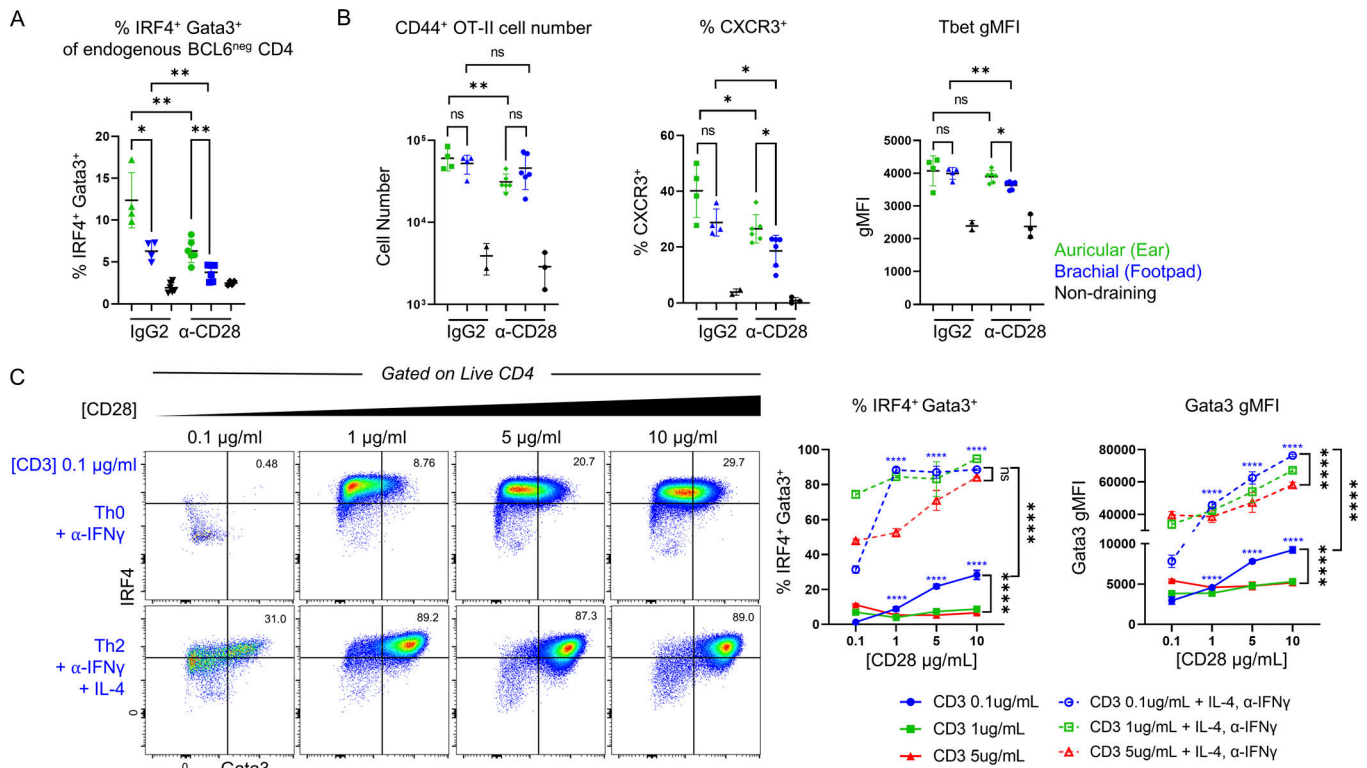
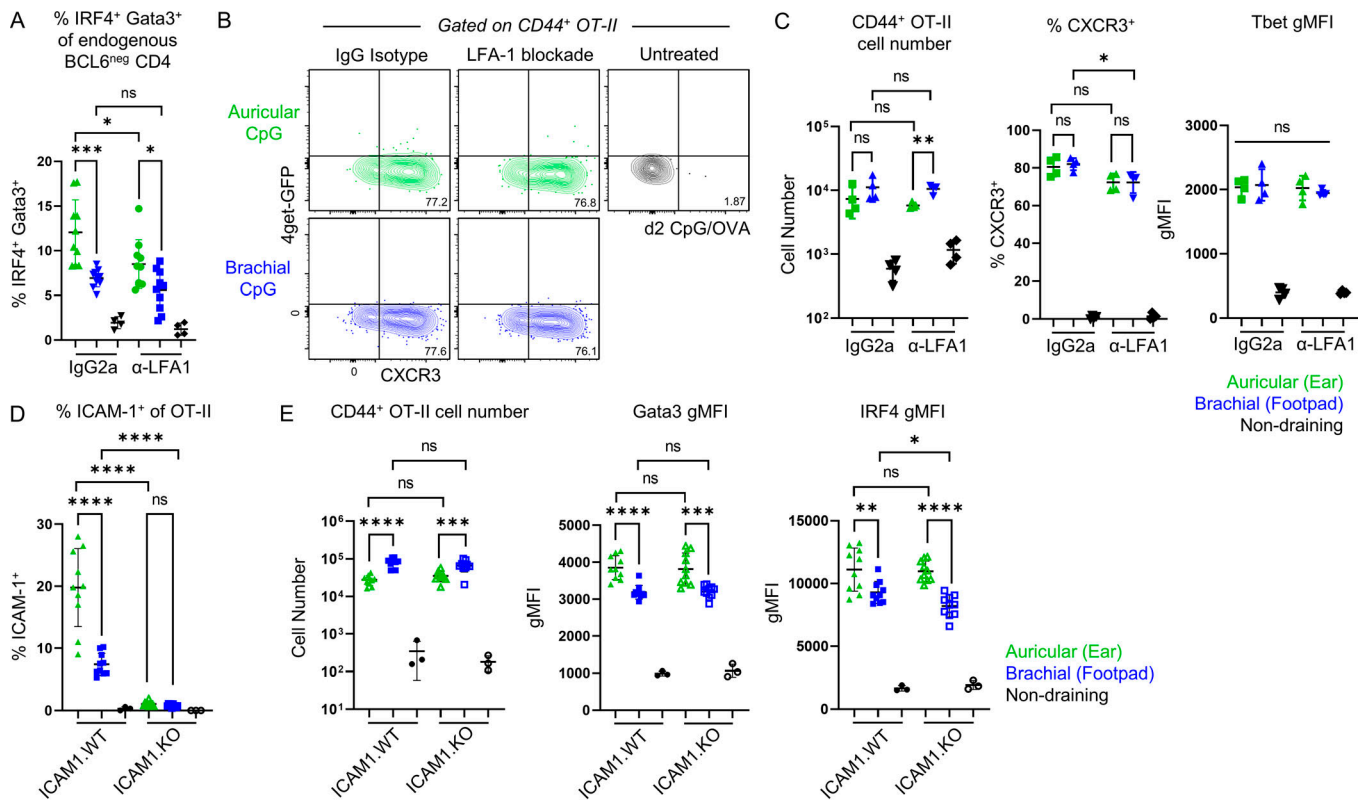


Figure S4. Role of CD28 in T helper cell responses. (A) Mice were transferred with naïve 4get.OT-II cells, treated with papain OVA as in Fig. 1 A, and administered α -CD28 blocking antibody or IgG isotype control intraperitoneally 24 h after immunization, and dLNs were harvested and assessed by flow cytometry at 48 h. Endogenous CD44⁺Ki67⁺BCL6⁻ CD4 T cells were assessed for Gata3 and IRF4 coexpression with the indicated treatment. **(B)** Naïve CD45.2 4get.OT-II cells were transferred to CD45.1 mice and injected with CpG OVA in the ear pinnae or front footpad. Mice were treated intraperitoneally with α -CD28 6 h post immunization, treated intraperitoneally with α -CD28 blocking antibody or IgG isotype control 24 h post immunization, and dLNs were harvested and assessed by flow cytometry at 48 h. Quantification of CD44⁺ OT-II cell number, frequency of CXCR3⁺ cells, and Tbet gMFI on CD44⁺ OT-II cells is shown. **(C)** Naïve OT-II cells were cultured in vitro with the indicated concentrations of α -CD3 and α -CD28. IL-4 and α -IFN γ were added to the culture in some conditions (dashed lines). Cells were harvested for flow cytometry 48 h later and assessed for expression of Gata3 and IRF4. Data shown represents one independent experiment with at least $n = 4$ independently immunized lymph nodes from two mice per group or three wells per treatment group. Graphs show mean \pm SD and were analyzed using unpaired Student's t test. **** $P < 0.0001$; *** $P < 0.001$; ** $P < 0.01$; * $P < 0.05$; $P > 0.05$ not significant (ns). Figures are representative of four independent experiments.



F Proposed model for initiation of Th2 differentiation in skin draining LNs

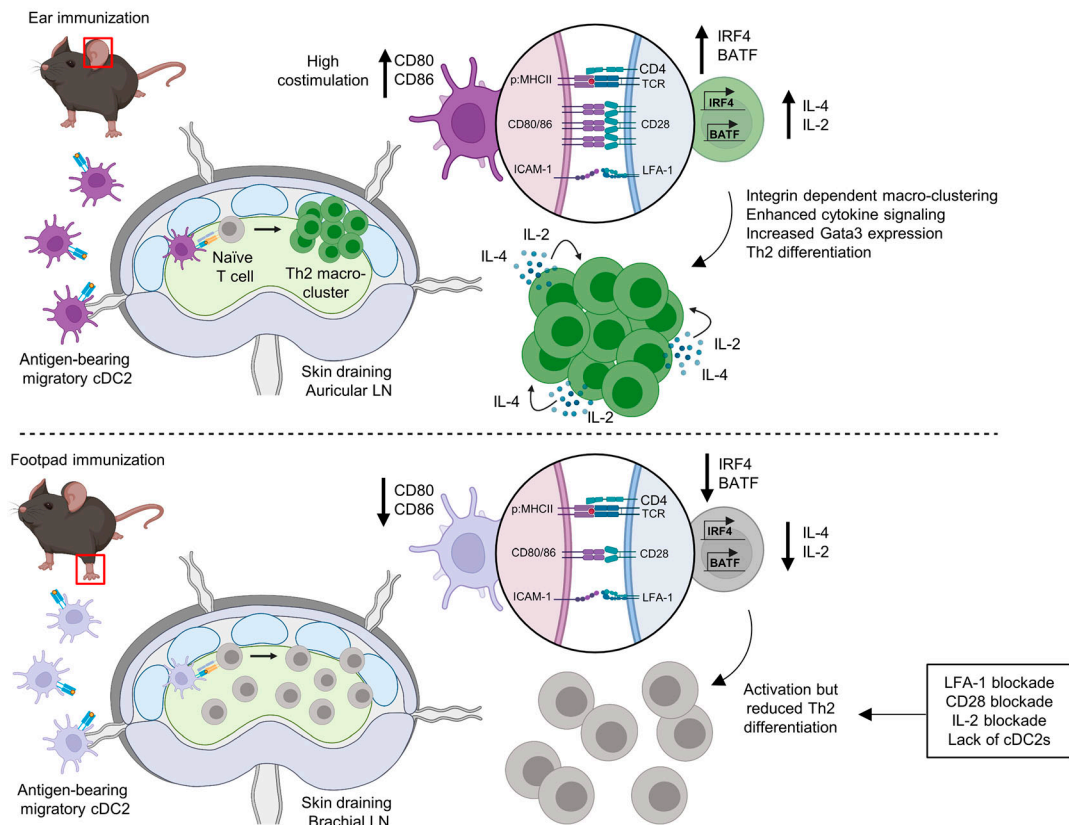


Figure S5. Role of LFA-1 in T helper cell responses. (A) Mice were transferred with naïve 4get.OT-II cells, treated with papain OVA as in Fig. 1 A, and administered α -LFA1 blocking antibody or IgG isotype control intraperitoneally 24 h after immunization and dLNs were harvested and assessed by flow cytometry at 48 h. Endogenous CD44⁺Ki67⁺BCL6⁻ CD4 T cells were assessed for Gata3 and IRF4 coexpression with the indicated treatment. (B and C) Naïve

CD45.2 4get.OT-II cells were transferred to CD45.1 mice and injected with CpG OVA in the ear pinnae or front footpad. Mice were treated intraperitoneally with α -CD62L 6 h after immunization, treated intraperitoneally with α -LFA1 blocking antibody or IgG isotype control 24 h after immunization, and dLNs were harvested and assessed by flow cytometry at 48 h. Representative plots (B) and quantification (C) of CD44⁺ OT-II cell number, frequency of CXCR3⁺ cells, and Tbet gMFI on CD44⁺ OT-II are shown. **(D and E)** Naïve ICAM-1.KO or ICAM-1.WT OT-II cells were transferred to CD45.1 B6 recipients and injected with papain OVA in the ear pinnae or front footpad, treated intraperitoneally with α -CD62L 6 h after immunization, and dLNs were harvested and assessed by flow cytometry at 48 h. **(D)** Frequency of ICAM-1 expression on OT-II cells from ICAM-1.WT and ICAM-1.KO mice. **(E)** Quantification of the number of CD44⁺ OT-II cells, and Gata3 and IRF4 gMFI of CD44⁺ OT-II cells of the indicated cell type. **(F)** Proposed model for initiation of Th2 differentiation in skin-draining LNs. Papain immunization of the skin elicits the maturation, costimulatory molecule expression, and migration of antigen-bearing cDC2 to draining LNs where they induce Th2 responses within dedicated microenvironments localized at the T–B border. Th2 differentiation is driven by prolonged T–DC contacts leading to T cell activation via low levels of pMHC and high levels of costimulatory molecules on cDC2s which subsequently drives integrin-mediated macro-clustering, efficient cytokine exchange, and localized Th2 differentiation. Certain skin sites, such as the paw, induce reduced expression of costimulatory molecules on migratory cDC2s which leads to T cell proliferation but reduced macro-clustering and Th2 differentiation within corresponding draining LNs. Data shown represents one independent experiment with at least $n = 4$ independently immunized lymph nodes from two mice per group. Graphs show mean \pm SD and were analyzed using unpaired Student's t test. **** $P < 0.0001$; *** $P < 0.001$; ** $P < 0.01$; * $P < 0.05$; $P > 0.05$ not significant (ns). WT = wild type; KO = knockout. A–C are representative of four independent experiments. D and E are representative of two independent experiments.